

Constrained Secrecy Capacity of Finite-Input Intersymbol Interference Wiretap Channels

Aria Nouri, *Student Member, IEEE*, Reza Asvadi, *Senior Member, IEEE*, Jun Chen, *Senior Member, IEEE*, and Pascal O. Vontobel, *Fellow, IEEE*

Abstract

We consider reliable and secure communication over intersymbol interference wiretap channels (ISI-WTCs). In particular, we first examine the setup where the source at the input of an ISI-WTC is unconstrained and then, based on a general achievability result for arbitrary wiretap channels, we derive an achievable secure rate for this ISI-WTC. Afterwards, we examine the setup where the source at the input of an ISI-WTC is constrained to be a finite-state machine source (FSMS) of a certain order and structure. Optimizing the parameters of this FSMS toward maximizing the secure rate is a computationally intractable problem in general, and so, toward finding a local maximum, we propose an iterative algorithm that at every iteration replaces the secure rate function by a suitable surrogate function whose maximum can be found efficiently. Although the secure rates achieved in the unconstrained setup are potentially larger than the secure rates achieved in the constraint setup, the latter setup has the advantage of leading to efficient algorithms for estimating achievable secure rates and also has the benefit of being the basis of efficient encoding and decoding schemes.

Index Terms

Intersymbol interference (ISI), intersymbol interference wiretap channel (ISI-WTC), finite-state machine channel (FSMC), finite-state machine source (FSMS), secure rate, optimization.

A. Nouri and R. Asvadi are with the Department of Telecommunications, Faculty of Electrical Engineering, Shahid Beheshti University, Tehran, Iran. (e-mails: ariya@ieee.org; r_asvadi@sbu.ac.ir) R. Asvadi is the corresponding author.

J. Chen is with the Department of Electrical and Computer Engineering, McMaster University, Hamilton, ON, Canada (e-mail: junchen@mail.ece.mcmaster.ca).

P.O. Vontobel is with the Department of Information Engineering and the Institute of Theoretical Computer Science and Communications, The Chinese University of Hong Kong, Hong Kong SAR (e-mail: pascal.vontobel@ieee.org).

The work described in this paper was partially supported by a grant from the Research Grants Council of Shahid Beheshti University, Tehran, Iran, and by a grant from the Research Grants Council of the Hong Kong Special Administrative Region, China (Project No. CUHK 14207518).

This paper was presented in part at the IEEE Information Theory Workshop, Kanazawa, Japan, Oct. 2021 [1].

I. INTRODUCTION

A. Motivation and System Model

The increasing number of connected users and the broadcasting nature of the wireless medium lead to a flurry of security challenges for wireless communication applications. For example, typical cryptographic protocols require significant communication resources for distributing and maintaining secret keys. This issue noticeably decreases the data transmission efficiency as the number of users gradually increases [2]. In addition, traditional cryptosystems rely on the assumption that eavesdroppers have limited computational power, making them vulnerable against more and more powerful (quantum) computers [3]. Alternatively, information-theoretic secrecy [4] utilizes the inherent randomness of communication channels (e.g., noise and interference) to achieve security at the physical layer [5], without requiring secret key agreement and without imposing any constraints on the eavesdroppers' computational power.

The emergence of different wireless applications gives rise to diverse channel models for various channel conditions. Intersymbol interference (ISI) channels, also known as partial-response channels [6, Ch. 9], are used as a model for high-data-rate transmission over wireless channels when the delay spread of the channel exceeds the symbol duration. This phenomenon in wireless propagation is also referred to as frequency-selective multipath fading [6]. In order to be specific, consider a multipath fading channel $Y(t_c) \triangleq \sum_{\ell=0}^{m_c} g_{c,\ell}(t_c)X(t_c - \tau_\ell) + N(t_c)$ with continuous-time variable $t_c \in \mathbb{R}$, where $X(t_c)$, $Y(t_c)$, and $N(t_c)$ denote the input, the output, and the additive noise signal, and where $g_{c,\ell}(t_c)$ and τ_ℓ are, respectively, the gain and the delay of the ℓ -th path, $0 \leq \ell \leq m_c$. When the symbol duration is smaller than $\tau_{m_c} - \tau_0$, the sampled output of a filter matched to the shaping pulse at the receiver leads to an ISI channel model. Such an ISI model usually appears in single-carrier communication systems, which require a higher power efficiency and a better peak-to-average power ratio (compared with multicarrier communication systems) and which appear in applications of the narrowband internet of things (NB-IoT)¹ [8] as outlined in specifications of 5G and beyond-5G networks [9], [10]. Note that ISI is also caused by multipath propagation in long-range underwater acoustic communications [11].

¹In typical applications of the NB-IoT, ISI is mitigated by appending a sufficiently large enough cyclic prefix to each transmitted block [7]. This method decreases the effective throughput as the delay spread of the channel increases.

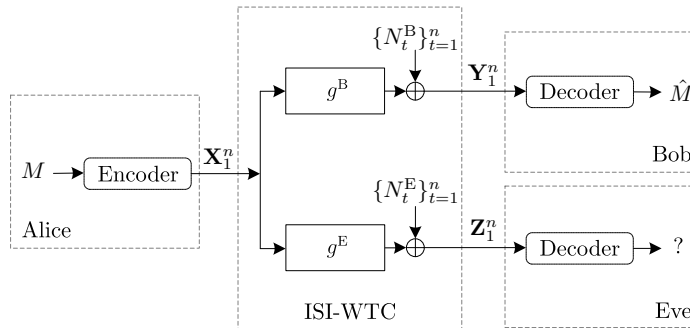


Fig. 1: Block diagram of the ISI-WTC.

Providing security at the physical layer of the above-mentioned communication technologies without imposing extra delay, power consumption, and processing burden, has received significant attention recently [12]–[14]. It is worthwhile to note that the NB-IoT mostly inherits the long-term evolution (LTE) infrastructure [9], and so the essential channels operate in the licensed sub-GHz spectrum range [15]. In this spectrum range, in contrast to the broadcasting applications in the THz carrier frequency range [16], one cannot choose the angular divergence of the transmitter beam to be sufficiently small toward preventing the eavesdropper from intercepting out-of-the-line-of-sight transmission signals. This issue presents a vulnerable environment at the physical layer of applications using the NB-IoT.

These considerations are motivating us to study theoretical aspects of the physical layer security over ISI wiretap channels (ISI-WTCs). As depicted in Fig. 1, the ISI-WTC comprises two ISI channels, where the primary channel connects a transmitter (called Alice) to a legitimate receiver (called Bob and abbreviated by “B”), and where the secondary channel connects the transmitter to an eavesdropper (called Eve and abbreviated by “E”). In order to focus on the key aspects of this setups, the channel gains are assumed to be constant and perfectly known to the receiver over each transmission block.²

B. Background, Related Works, and Contributions

ISI channels with finite memory length and finite input alphabets are a particular case of finite-state machine channels (FSMCs) [18]. Toward maximizing the achievable information rates over FSMCs, the classical Blahut-Arimoto algorithm (BAA) [19], [20] was generalized

²These assumptions are well established in slowly-varying channels and appear also in other studies of ISI channels (see, e.g., [17]).

in [21] to optimize finite-state machine sources (FSMSs) at the input of FSMCs. Comparing lower bounds on the capacity of FSMCs (i.e., the maximized achievable information rates) [21], [22] with the corresponding upper bounds [23], [24], typically shows a small gap between them, which can be further narrowed by increasing the memory order of the employed FSMS at the input [25].

Recently, Han and Sasaki [26], [27] derived the secrecy capacity of memoryless wiretap channels with both causal and non-causal channel state information at the encoder. Dai *et al.* [28] applied these results to physically degraded Gaussian wiretap channels with a noiseless private feedback from Bob's observations to the encoder. It was shown in [28] that the considered feedback enhances the secrecy capacity under the weak secrecy criterion. The delayed version of this feedback is employed in [29] to enlarge the rate-equivocation region of finite-state Markov wiretap channels.³ Additionally, as done for ISI channels in [30] and [31], the efficiency of secure communication in the physical layer can be enhanced by injecting cooperative artificial noise toward degrading Eve's channel while minimizing the impact on Bob's channel.

Due to power efficiency requirements, artificial-noise-aided communication has not received too much attention in recent technologies. Also, establishing a private noiseless channel to feed back the complete output of Bob's channel to Alice's encoder imposes a tremendous delay and processing overload on the higher layers of large cooperative networks. Therefore, we focus on the standard version of ISI-WTCs (with neither feedback nor additional artificial noise), as it requires few assumptions and consequently is more practically relevant.

In terms of the main focus of this paper, estimating the secrecy capacity of a finite-state wiretap channel was already considered in [32].⁴ However, the channel setup and the approach to estimate the secrecy capacity in [32] have the following limitations and weaknesses. Firstly, the assumptions for the channel setup in [32] resemble the general

³A finite-state Markov wiretap channel as in [29] is a wiretap channel where Bob's channel and Eve's channel are FSMCs where the (joint) state process is assumed to be a stationary ergodic Markov chain independent of the transmitted message.

⁴Note that in [32] a finite-state wiretap channel is defined to be a wiretap channel where Bob and Eve observe the input source through two distinct FSMCs.

assumptions for discrete memoryless wiretap channels in [33], where Eve’s channel is assumed to be noisier than Bob’s channel. However, as we will show, these assumptions are inadequate for ISI channels (and more generally, for FSMCs) due to the non-flat frequency responses of these channels. Secondly, the function that is used for approximating the secure rate function has the property that its gradient is usually not the same as the gradient of the secure rate function at a given operating point. This issue leads to an inaccurate search direction and eventually makes the algorithm unstable.

In the following, we highlight the main contributions and results presented in this paper.

- We consider an ISI-WTC where the input symbols are limited to some finite alphabet. In a first step, we derive the achievable secure rates for the *unconstrained* setup, i.e., the setup where no constraints are placed on the input distribution.
- We then consider the *constrained* setup, i.e., the setup where Alice’s source is an FSMS, resembling a Markov source of a specific order. Note that employing Markov sources at the input of ISI channels has the benefit of leading to efficient algorithms for estimation [34] and maximization [21] of information rates, approaching the capacity in point-to-point setups [25], and being a basis for efficient encoding and decoding schemes [35], [36]. Accordingly, we propose an efficient algorithm for optimizing FSMSs toward maximizing the obtained achievable secure rates over ISI-WTCs.
- Maximizing the above-mentioned secure rate is challenging because it is not a closed-form function of the input distribution, i.e., its evaluation is only possible through Monte-Carlo simulations. The key idea behind the proposed algorithm is to approximate the secure rate function by suitable surrogate functions that are well defined over a given polytope and can relatively easily be maximized. The proposed algorithm resembles the well-known expectation-maximization (EM) algorithm and has a similar convergence behavior when finding a local maximum. Let us emphasize that a benefit of our approach is that the optimization algorithm not only takes (estimated) zeroth-order information of the secure rate function into account, but also some (estimated) first-order information.
- We provide examples where the capacity of Eve’s channel is higher than the capacity of Bob’s channel, yet a nonzero secure rate is possible. These examples show that it is feasible to optimize FSMSs such that spectral discrepancies between the frequency re-

sponses of Bob’s channel and Eve’s channel can be exploited—without any further power consumption for transmitting interfering artificial noise toward jamming Eve’s channel.

The remainder of this paper is organized as follows. Section II introduces the system model and some preliminary concepts related to FSMSs, FSMCs, and ISI-WTCs. Section III-A gives a concise discussion about the employed secrecy criterion, based on which Section III-B presents achievability results of the (unconstrained and constrained) secure rates over ISI-WTCs. Section III-C discusses an efficient algorithm for estimating the secure rate achieved by a given FSMS at the input of an ISI-WTC. Section IV describes the proposed algorithm for optimizing the FSMS at the input of an ISI-WTC and analyzes it in detail. Section V contains some numerical results and discussions. Finally, Section VI draws the conclusions.

C. Notation

The sets of integers and complex numbers are denoted by \mathbb{Z} and \mathbb{C} , respectively. The ring of polynomials with coefficients in \mathbb{C} and indeterminate D is denoted by $\mathbb{C}[D]$. (“ D ” can be thought of as standing for “delay”.) Sets are denoted by calligraphic letters, e.g., \mathcal{S} . The Cartesian product of two sets \mathcal{X} and \mathcal{Y} is written as $\mathcal{X} \times \mathcal{Y}$, and the n -fold Cartesian product of \mathcal{X} with itself is written as \mathcal{X}^n . If \mathcal{X} is a finite set, then its cardinality is denoted by $|\mathcal{X}|$.

Random variables are denoted by upper-case italic letters, e.g., X , their realizations by the corresponding lower-case letters, e.g., x , and the set of possible values by the corresponding calligraphic letter, e.g., \mathcal{X} . Random vectors are denoted by upper-case boldface letters, e.g., \mathbf{X} , and their realizations by the corresponding lower-case letters, e.g., \mathbf{x} . For integers n_1 and n_2 satisfying $n_1 \leq n_2$, the notation $\mathbf{X}_{n_1}^{n_2} \triangleq (X_{n_1}, X_{n_1+1}, \dots, X_{n_2})$ is used for a time-indexed vector of random variables and $\mathbf{x}_{n_1}^{n_2} \triangleq (x_{n_1}, x_{n_1+1}, \dots, x_{n_2})$ for its realization. Boldface letters are also used for matrices, e.g., \mathbf{A} , with the (i, j) -entry of \mathbf{A} being called A_{ij} .

The probability of an event ξ is denoted by $\Pr(\xi)$. Furthermore, $p_X(\cdot)$ denotes the probability mass function (PMF) of X if X is a discrete random variable and the probability density function (PDF) of X if X is a continuous random variable. Similarly, $p_{Y|X}(\cdot|x)$ denotes the conditional PMF of Y given $X = x$ if Y is a discrete random variable and the conditional PDF of Y given $X = x$ if Y is a continuous random variable.

For any real number x , the expression $(x)^+$ stands for $\max\{x, 0\}$; similarly, $f^+(\cdot)$ stands for $(f(\cdot))^+$. Moreover, the expression $\log(\cdot)$ denotes the natural logarithm function.

The entropy of a random variable X , the mutual information between two random variables X and Y , and the mutual information between two random variables X and Y conditioned on the random variable Z are denoted by $H(X)$, $I(X; Y)$, and $I(X; Y|Z)$, respectively. The *mutual information density* between the respective realizations of random variables X and Y is defined to be $i(x; y) \triangleq \log\left(\frac{p_{X,Y}(x,y)}{p_X(x) \cdot p_Y(y)}\right)$. Moreover, the *conditional mutual information density* between the respective realizations of random variables X and Y given $Z = z$ is defined to be $i(x; y|z) \triangleq \log\left(\frac{p_{X,Y|Z}(x,y|z)}{p_{X|Z}(x|z) \cdot p_{Y|Z}(y|z)}\right)$. Consequently, we have $I(X; Y) = \sum_{x,y} p_{X,Y}(x,y) \cdot i(x; y)$, and also $I(X; Y|Z) = \sum_{x,y,z} p_{X,Y,Z}(x,y,z) \cdot i(x; y|z)$. Finally, the variational distance between the PMFs of two random variables X and Y over the same finite alphabet \mathcal{X} is defined as $d_{\mathcal{X}}(p_X, p_Y) \triangleq \sum_{x \in \mathcal{X}} |p_X(x) - p_Y(x)|$.

II. PRELIMINARIES AND DEFINITIONS

This section gives the definitions of finite-state machine sources (FSMSs) and finite-state machine channels (FSMCs) along with special cases as far as relevant for this paper. Based on these definitions, we introduce the finite-state joint source-wiretap channels (FS-JSWTCs), which is the key element for studying FSMSs at the input of ISI-WTCs. The interested reader is referred to [18], [21] for more background and further examples.

Definition 1 (Finite-State Machine Source (FSMS)). A discrete-time, time-invariant FSMS has a state process $\{\bar{S}_t\}_{t \in \mathbb{Z}}$ and an output process $\{X_t\}_{t \in \mathbb{Z}}$, where $\bar{S}_t \in \bar{\mathcal{S}}$ and $X_t \in \mathcal{X}$ for all $t \in \mathbb{Z}$. We assume that the alphabets $\bar{\mathcal{S}}$ and \mathcal{X} are finite and that for any positive integer n the joint PMF of $\bar{\mathbf{S}}_1^n$ and \mathbf{X}_1^n conditioned on $\bar{S}_0 = \bar{s}_0$ decomposes as $p_{\mathbf{X}_1^n, \bar{\mathbf{S}}_1^n | \bar{S}_0}(\mathbf{x}_1^n, \bar{\mathbf{s}}_1^n | \bar{s}_0) = \prod_{t=1}^n p_{X_t, \bar{S}_t | \bar{S}_{t-1}}(x_t, \bar{s}_t | \bar{s}_{t-1})$, where $p_{X_t, \bar{S}_t | \bar{S}_{t-1}}(x_t, \bar{s}_t | \bar{s}_{t-1})$ is independent of t . \square

Remark 1. We will mostly consider FSMSs where $\bar{s}_t \triangleq \mathbf{x}_{t-\bar{\nu}}^t$ ($\bar{\mathcal{S}} \triangleq \mathcal{X}^{\bar{\nu}}$) for all $t \in \mathbb{Z}$ and for some positive $\bar{\nu} \in \mathbb{Z}$ (called the memory order of such an FSMS). Considering $\bar{s}_{t-1} = \mathbf{x}_{t-\bar{\nu}}^{t-1}$ and $\bar{s}_t = \mathbf{x}_{t-\bar{\nu}}^t$, it holds that $p_{X_t, \bar{S}_t | \bar{S}_{t-1}}(x_t, \bar{s}_t | \bar{s}_{t-1}) = p_{X_t | X_{t-\bar{\nu}}^{t-1}}(x_t | \mathbf{x}_{t-\bar{\nu}}^{t-1})$. Given the initial state $\bar{S}_0 = \bar{s}_0$, this implies a bijection between the source state sequence and the source output sequence, i.e., the state sequence $\bar{\mathbf{s}}_1^n$ uniquely determines the output sequence \mathbf{x}_1^n and vice versa. Obviously, such an FSMS is characterized by the triple $(\mathcal{X}, \bar{\nu}, p_{X_t | X_{t-\bar{\nu}}^{t-1}}(x_t | \mathbf{x}_{t-\bar{\nu}}^{t-1}))$. \square

Note that all possible state sequences of an FSMS can be represented by a trellis diagram. Because of the assumed time-invariance, it is sufficient to show a single trellis section. For example, Fig. 2(a) shows a trellis section corresponding to an FSMS characterized by the triple $(\mathcal{X} \triangleq \{+1, -1\}, \bar{\nu} \triangleq 3, p_{X_t|X_{t-\bar{\nu}}}(x_t|\mathbf{x}_{t-\bar{\nu}}^{t-1})$.

Before giving the definition of an ISI channel we introduce the more general class of finite-state machine channels (which were called finite-state channels in [18]).

Definition 2 (Finite-State Machine Channel (FSMC)). A discrete-time, time-invariant FSMC has an input process $\{X_t\}_{t \in \mathbb{Z}}$, an output process $\{Y_t\}_{t \in \mathbb{Z}}$, and a state process $\{S'_t\}_{t \in \mathbb{Z}}$, where $X_t \in \mathcal{X}$, $Y_t \in \mathcal{Y}$, and $S'_t \in \mathcal{S}'$ for all $t \in \mathbb{Z}$. We assume that the alphabets \mathcal{X} and \mathcal{S}' are finite and that for any positive integer n the joint PMF/PDF of \mathbf{S}'_1^n and \mathbf{Y}_1^n conditioned on $S'_0 = s'_0$ and $\mathbf{X}_1^n = \mathbf{x}_1^n$ is $p_{\mathbf{S}'_1^n, \mathbf{Y}_1^n | S'_0, \mathbf{X}_1^n}(s'_1, \mathbf{y}_1^n | s'_0, \mathbf{x}_1^n) = \prod_{t=1}^n p_{S'_t, Y_t | S'_{t-1}, X_t}(s'_t, y_t | s'_{t-1}, x_t)$, where $p_{S'_t, Y_t | S'_{t-1}, X_t}(s'_t, y_t | s'_{t-1}, x_t)$ is independent of t . \square

An important special case of an FSMC is an ISI channel.

Definition 3 (Intersymbol Interference (ISI) Channel). An ISI channel with transfer polynomial $g(D) \triangleq \sum_{t=0}^m g_t D^t \in \mathbb{C}[D]$ with $g_m \neq 0$, where m is called the memory length, has an input process $\{X_t\}_{t \in \mathbb{Z}}$, a noiseless output process $\{U_t\}_{t \in \mathbb{Z}}$ with $U_t \triangleq \sum_{\ell=0}^m g_\ell X_{t-\ell}$, a noise process $\{N_t\}_{t \in \mathbb{Z}}$, and a noisy output process $\{Y_t\}_{t \in \mathbb{Z}}$ with $Y_t \triangleq U_t + N_t$, where $X_t, U_t, N_t, Y_t \in \mathbb{C}$ for all $t \in \mathbb{Z}$, and where the noise process is independent of the channel input process. In the following, we will assume that the noise process is white Gaussian noise, i.e., $\{N_t\}_{t \in \mathbb{Z}}$ are i.i.d. Gaussian random variables with mean zero and variance σ^2 . Clearly, an ISI channel is parameterized by the couple $(g(D), \sigma^2)$. \square

An ISI channel described by the couple $(g(D) \triangleq \sum_{t=0}^m g_t D^t, \sigma^2)$, where $m < \infty$, and having an input process $\{X_t\}_{t \in \mathbb{Z}}$ taking values in a finite set $\mathcal{X} \subsetneq \mathbb{C}$ is a special case of an FSMC. Indeed, let $\mathcal{S}' \triangleq \mathcal{X}^m$. Then $p_{S'_t, Y_t | S'_{t-1}, X_t}(s'_t, y_t | s'_{t-1}, x_t) = p_{S'_t | S'_{t-1}, X_t}(s'_t | s'_{t-1}, x_t) \cdot p_{Y_t | S'_{t-1}, X_t}(y_t | s'_{t-1}, x_t)$, where

$$p_{S'_t | S'_{t-1}, X_t}(s'_t | s'_{t-1}, x_t) \triangleq \begin{cases} 1 & \text{(if } s'_t = \mathbf{x}_{t-m+1}^t \text{ and } s'_{t-1} = \mathbf{x}_{t-m}^{t-1}) \\ 0 & \text{(otherwise)} \end{cases},$$

$$p_{Y_t | S'_{t-1}, X_t}(y_t | s'_{t-1}, x_t) \triangleq \frac{1}{2\pi\sigma^2} \cdot \exp\left(-\frac{|y_t - u_t|^2}{2\sigma^2}\right) \quad \left(\text{if } s'_{t-1} = \mathbf{x}_{t-m}^{t-1} \in \mathcal{X}^m \text{ and } u_t = \sum_{\ell=0}^m g_\ell x_{t-\ell}\right).$$

All possible state sequences of an ISI channel (and more generally, of an FSMC) can be represented by a trellis diagram. Because of the assumed time-invariance, it is sufficient to show a single trellis section. For example, Fig. 2(b) shows a trellis section of an ISI channel characterized by the couple $(g(D) \triangleq 1 - D, \sigma^2)$, known as a dicode channel, with an input alphabet $\mathcal{X} \triangleq \{+1, -1\}$. In this diagram, branches start at state $s'_{t-1} = x_{t-1}$, end at state $s'_t = x_t$, and have noiseless channel output symbol $u_t = x_t - x_{t-1}$ shown next to them.

Definition 4 (Intersymbol Interference Wiretap Channel (ISI-WTC)). In an ISI-WTC, Alice transmits data symbols over Bob's channel and over Eve's channel, which are both assumed to be ISI channels with finite input alphabet $\mathcal{X} \subsetneq \mathbb{C}$. Specifically, Bob's channel is an ISI channel described by the couple $(g^B(D), \sigma_B^2)$, with transfer polynomial $g^B(D) = \sum_{t=0}^{m_B} g_t^B D^t$, noiseless output process $\{U_t\}_{t \in \mathbb{Z}}$, noise process $\{N_t^B\}_{t \in \mathbb{Z}}$, and noisy output process $\{Y_t\}_{t \in \mathbb{Z}}$. Similarly, Eve's channel is an ISI channel described by the couple $(g^E(D), \sigma_E^2)$, with transfer polynomial $g^E(D) = \sum_{t=0}^{m_E} g_t^E D^t$, noiseless output process $\{V_t\}_{t \in \mathbb{Z}}$, noise process $\{N_t^E\}_{t \in \mathbb{Z}}$, and noisy output process $\{Z_t\}_{t \in \mathbb{Z}}$. We assume that the noise process of Bob's channel and the noise process of Eve's channel are independent. Clearly, the ISI-WTC is parameterized by the quadruple $(g^B(D), g^E(D), \sigma_B^2, \sigma_E^2)$. \square

Definition 5 (Finite-State Joint Source Wiretap Channel (FS-JSWTC)). An FS-JSWTC is a discrete-time, time-invariant finite-state machine resulting from the concatenation of an FSMS (as in Remark 1) described by $(\mathcal{X}, \bar{\nu}, p_{X_t|X_{t-\bar{\nu}}}(x_t|\mathbf{x}_{t-\bar{\nu}}^{t-1}))$ and an ISI-WTC (as in Definition 4) described by $(g^B(D), g^E(D), \sigma_B^2, \sigma_E^2)$. Let $\nu \triangleq \max(\bar{\nu}, m_B, m_E)$ be the memory order of the FS-JSWTC, where m_B and m_E are the degrees of $g^B(D)$ and $g^E(D)$, respectively. Accordingly, the state space of this FS-JSWTC is given by $\mathcal{S} \triangleq \mathcal{X}^\nu$ and the state at time t is given by $s_t \triangleq \mathbf{x}_{t-\nu+1}^t$ for all $t \in \mathbb{Z}$. \square

In the following, we consider FSMSs with $\bar{\nu} \geq m_B$ and $\bar{\nu} \geq m_E$, which implies $\nu = \max(\bar{\nu}, m_B, m_E) = \bar{\nu}$.⁵ Hence, the state transition probabilities of the finite-state machine underlying the FS-JSWTC will be the same as the state transition probabilities of the FSMS.

Definition 6. Let \mathcal{B} denote the set of all valid consecutive state pairs $(s_{t-1}, s_t) \in \mathcal{S} \times \mathcal{S}$ for

⁵With suitable adaptations, FSMSs with $\bar{\nu} < \max(m_B, m_E)$ can be handled.

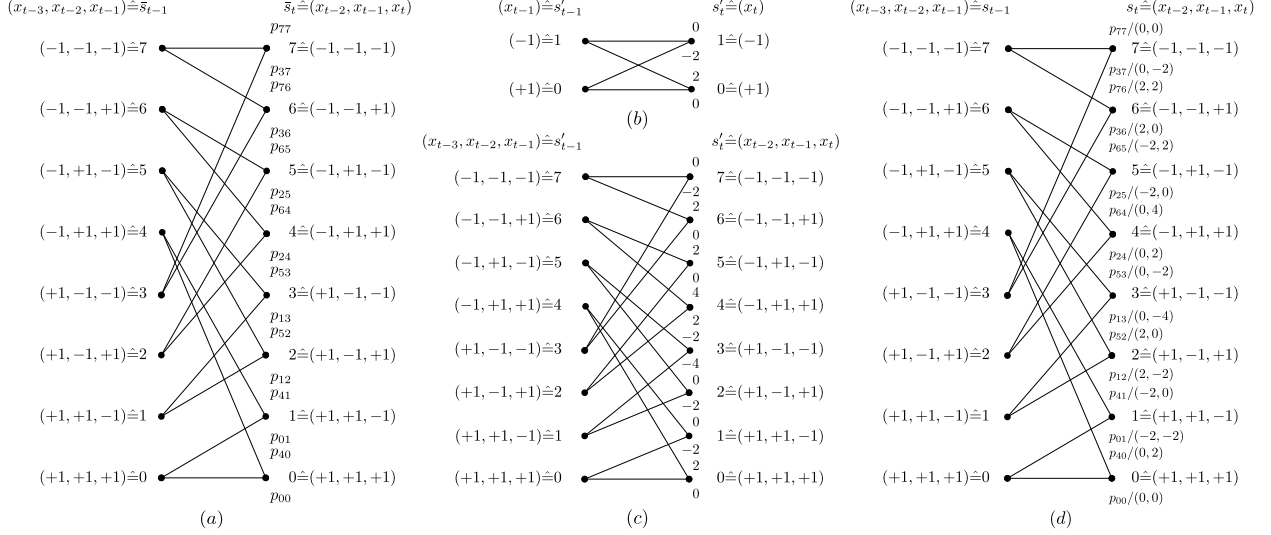


Fig. 2: (a) Trellis section of an FSMS with $\mathcal{X} = \{+1, -1\}$ and memory order $\bar{\nu} = 3$. State transition probabilities are shown next to branches. (b) Trellis section of a dicode channel (i.e., an ISI channel with $g(D) = 1 - D$) when used with input alphabet $\mathcal{X} = \{+1, -1\}$. The noiseless channel output symbol is shown next to branches. (c) Trellis section of an EPR4 channel (i.e., an ISI channel with $g(D) = 1 + D - D^2 - D^3$) when used with input alphabet $\mathcal{X} = \{+1, -1\}$. The noiseless channel output symbol is shown next to branches. (d) Trellis section of an FS-JSWTC comprised of a third-order FSMS, a dicode channel to Bob, and an EPR4 channel to Eve. State transition probabilities and noiseless channel output symbols (one noiseless channel output symbol for Bob's channel, one noiseless channel output symbol for Eve's channel) are shown next to branches.

any $t \in \mathbb{Z}$. Moreover, let $\vec{\mathcal{S}}_i \triangleq \{j \mid (i, j) \in \mathcal{B}\}$ be the set of states S_t reachable from the state $S_{t-1} = i$, and $\overleftarrow{\mathcal{S}}_j \triangleq \{i \mid (i, j) \in \mathcal{B}\}$ be the set of states S_{t-1} that can reach $S_t = j$. \square

Definition 7. For every $(i, j) \in \mathcal{B}$, let $p_{ij} \triangleq p_{S_t|S_{t-1}}(j|i)$ be the time-invariant state transition probability assigned by an ergodic and non-periodic FSMS. Then there is a unique stationary state PMF $\{\mu_i\}_{i \in \mathcal{S}}$ such that $p_{S_t}(i) = \mu_i$ for all $t \in \mathbb{Z}$, $i \in \mathcal{S}$. Finally, let $Q_{ij} \triangleq \mu_i \cdot p_{ij}$, for all $(i, j) \in \mathcal{B}$. \square

In the above definition, we started with $\{p_{ij}\}_{(i,j) \in \mathcal{B}}$ and derived $\{\mu_i\}_{i \in \mathcal{S}}$ and $\{Q_{ij}\}_{(i,j) \in \mathcal{B}}$ from $\{p_{ij}\}_{(i,j) \in \mathcal{B}}$. However, for analytical purposes, it turns out to be beneficial to start with $\{Q_{ij}\}_{(i,j) \in \mathcal{B}}$ and derive $\{p_{ij}\}_{(i,j) \in \mathcal{B}}$ and $\{\mu_i\}_{i \in \mathcal{S}}$ from $\{Q_{ij}\}_{(i,j) \in \mathcal{B}}$. Note that the set of all valid $\{Q_{ij}\}_{(i,j) \in \mathcal{B}}$ for a fixed set \mathcal{B} is given by the polytope $\mathcal{Q}(\mathcal{B})$, where

$$\mathcal{Q}(\mathcal{B}) \triangleq \left\{ \{Q_{ij}\}_{(i,j) \in \mathcal{B}} \mid Q_{ij} \geq 0, \forall (i, j) \in \mathcal{B}; \sum_{(i,j) \in \mathcal{B}} Q_{ij} = 1; \sum_{j \in \vec{\mathcal{S}}_i} Q_{ij} = \sum_{k \in \overleftarrow{\mathcal{S}}_i} Q_{ki}, \forall i \in \mathcal{S} \right\}.$$

(See [21] for similar observations.) In the following, we will use the short-hand notation \mathbf{Q} for $\{Q_{ij}\}_{(i,j) \in \mathcal{B}}$. Moreover, similar to [21, Assumption 34], we will only be interested in

sets \mathcal{B} where the FSMSs corresponding to the relative interior of $\mathcal{Q}(\mathcal{B})$ are ergodic and non-periodic.

Example 1. Consider an FS-JSWTC, where the FSMS is described by $(\mathcal{X}, \bar{\nu}, p_{X_t|X_{t-\bar{\nu}}}(x_t|\mathbf{x}_{t-\bar{\nu}}^{t-1}))$ with $\mathcal{X} = \{+1, -1\}$ and $\bar{\nu} = 3$ (see Fig. 2(a)), where Bob's channel is a dicode channel, i.e., $g^B(D) = 1 - D$ (see Fig. 2(b)), and where Eve's channel is an EPR4 channel, i.e., $g^E(D) = 1 + D - D^2 - D^3$ (see Fig. 2(c)). All possible state sequences of an FS-JSWTC can be represented by a trellis diagram. Because of the assumed time-invariance, it is sufficient to show a single trellis section, as shown in Fig. 2(d) for the present example. \square

Remark 2 (Parameterized family of \mathbf{Q}). Frequently, we will consider $\mathbf{Q}(\theta)$, i.e., the setup where \mathbf{Q} is a function of some parameter θ . More precisely, for every $(i, j) \in \mathcal{B}$, we let $Q_{ij}(\theta)$ be a smooth function of the parameter θ , where θ varies over a suitable range. We require for every θ that it holds that $\mathbf{Q}(\theta) = \{Q_{ij}(\theta)\}_{(i,j) \in \mathcal{B}} \in \mathcal{Q}(\mathcal{B})$. Moreover, for every $(i, j) \in \mathcal{B}$, we denote the derivative of $Q_{ij}(\theta)$ w.r.t. θ and evaluated at $\tilde{\theta}$ by $Q_{ij}^\theta(\tilde{\theta})$. We denote the corresponding steady-state and state transition probabilities parameterized by θ by $\mu_i(\theta)$ and $p_{ij}(\theta)$, respectively. Similarly, we denote their derivatives w.r.t. θ and evaluated at $\tilde{\theta}$ by $\mu_i^\theta(\tilde{\theta})$ and $p_{ij}^\theta(\tilde{\theta})$, respectively. Because $\mathbf{Q}(\theta) \in \mathcal{Q}(\mathcal{B})$, we have $\sum_{(i,j) \in \mathcal{B}} Q_{ij}^\theta(\tilde{\theta}) = 0$ and $\sum_{i \in \mathcal{S}} \mu_i^\theta(\tilde{\theta}) = 0$. \square

III. SECURE RATE: ACHIEVABILITY AND ESTIMATION

This section is structured as follows. In Section III-A we discuss the secrecy criterion that is used in this paper, in Section III-B we establish a lower bound on the achievable secure rates over ISI-WTCs, and finally, in Section III-C, we present numerical estimates of the obtained secure rates.

A. Secrecy Criterion

Let M be a random variable corresponding to a uniformly chosen secret message from an alphabet \mathcal{M} . (Note that \mathcal{M} implicitly depends on the block length n .) Moreover, recall that the sequence observed by Eve is denoted by \mathbf{Z}_1^n (see Fig. 1). The statistical dependence between M and \mathbf{Z}_1^n is often measured in terms of the mutual information between M and \mathbf{Z}_1^n to ensure the information-theoretic perfect secrecy. For instance, the so-called strong secrecy

criterion [37] requires $I(M; \mathbf{Z}_1^n) < \delta_n$ and the so-called weak secrecy criterion [38] requires $\frac{1}{n}I(M; \mathbf{Z}_1^n) < \delta_n$ for some suitably small $\delta_n \geq 0$. (See also the recent survey paper [4].)

On one hand, the weak secrecy criterion is easier to achieve, but it might lead to coding schemes that are vulnerable for practical purposes [39, Ch. 3.3]. On the other hand, the strong secrecy criterion is much more desirable, but very difficult to achieve with practical coding schemes [40]. Therefore, in the following we will use a secrecy criterion that is stronger than the weak secrecy criterion, but more easily achieved than the strong secrecy criterion [40, Proposition 1]. Namely, we will use the following secrecy criterion based on the variational distance $d_{\mathcal{M} \times \mathcal{Z}^n}(p_{M, \mathbf{Z}_1^n}, p_M p_{\mathbf{Z}_1^n})$:

$$d_{\mathcal{M} \times \mathcal{Z}^n}(p_{M, \mathbf{Z}_1^n}, p_M p_{\mathbf{Z}_1^n}) < \delta_n \quad \text{for some suitably small } \delta_n \geq 0. \quad (1)$$

Note that $d_{\mathcal{M} \times \mathcal{Z}^n}(p_{M, \mathbf{Z}_1^n}, p_M p_{\mathbf{Z}_1^n})$, which was called $\mathbb{S}_2(p_{M, \mathbf{Z}_1^n}, p_M p_{\mathbf{Z}_1^n})$ in [40], can be bounded as

$$\begin{aligned} d_{\mathcal{M} \times \mathcal{Z}^n}(p_{M, \mathbf{Z}_1^n}, p_M p_{\mathbf{Z}_1^n}) &= \int_{\mathbf{z}_1^n \in \mathcal{Z}^n} \sum_{m \in \mathcal{M}} p_M(m) \cdot \left| p_{\mathbf{z}_1^n | M}(\mathbf{z}_1^n | m) - \sum_{\tilde{m} \in \mathcal{M}} p_{\mathbf{z}_1^n, M}(\mathbf{z}_1^n, \tilde{m}) \right| d\mathbf{z}_1^n \\ &\leq \sum_{(m, \tilde{m}) \in \mathcal{M}^2} p_M(m) \cdot p_M(\tilde{m}) \cdot \int_{\mathbf{z}_1^n \in \mathcal{Z}^n} \left| p_{\mathbf{z}_1^n | M}(\mathbf{z}_1^n | m) - p_{\mathbf{z}_1^n | M}(\mathbf{z}_1^n | \tilde{m}) \right| d\mathbf{z}_1^n \\ &= \sum_{(m, \tilde{m}) \in \mathcal{M}^2} p_M(m) \cdot p_M(\tilde{m}) \cdot d_{\mathcal{Z}^n}(p_{\mathbf{z}_1^n | M=m}, p_{\mathbf{z}_1^n | M=\tilde{m}}), \end{aligned} \quad (2)$$

where the inequality follows from the triangle inequality. It follows from (2) that satisfying (1) makes $m, \tilde{m} \in \mathcal{M}$ statistically (almost) indistinguishable at Eve's decoder.

For further context, note that the criterion in (1) is weaker than the so-called distinguishing secrecy criterion in cryptography [41], which requires $\max_{(m, \tilde{m}) \in \mathcal{M}^2} (d_{\mathcal{Z}^n}(p_{\mathbf{z}_1^n | M=m}, p_{\mathbf{z}_1^n | M=\tilde{m}})) < \delta_n$ for some suitably small $\delta_n \geq 0$, and which is equivalent to the so-called the semantic secrecy criterion, which requires that it is impossible for Eve to estimate any function of M better than to guess it without considering \mathbf{Z}_1^n [41].

B. Secure Rate: Achievability

Following [42], the spectral sup/inf-mutual information rates are defined to be

$$\text{p-lim sup}_{n \rightarrow \infty} \frac{1}{n} i(\mathbf{X}_1^n; \mathbf{Y}_1^n) \triangleq \inf \left\{ \alpha : \lim_{n \rightarrow \infty} \Pr \left(\frac{1}{n} i(\mathbf{X}_1^n; \mathbf{Y}_1^n) > \alpha \right) = 0 \right\},$$

$$\text{p-lim inf}_{n \rightarrow \infty} \frac{1}{n} i(\mathbf{X}_1^n; \mathbf{Y}_1^n) \triangleq \sup \left\{ \beta : \lim_{n \rightarrow \infty} \Pr \left(\frac{1}{n} i(\mathbf{X}_1^n; \mathbf{Y}_1^n) < \beta \right) = 0 \right\}.$$

Lemma 1. [43, Lemma 2] For an arbitrary wiretap channel $(\mathcal{X}, \{p_{\mathbf{Y}_1^n, \mathbf{Z}_1^n | \mathbf{X}_1^n}(\mathbf{y}_1^n, \mathbf{z}_1^n | \mathbf{x}_1^n)\}_{n=1}^\infty, \mathcal{Y}, \mathcal{Z})$ consisting of an arbitrary input alphabet \mathcal{X} , two arbitrary output alphabets \mathcal{Y} and \mathcal{Z} corresponding to Bob's and Eve's observations, respectively, and a sequence of transition probabilities $\{p_{\mathbf{Y}_1^n, \mathbf{Z}_1^n | \mathbf{X}_1^n}(\mathbf{y}_1^n, \mathbf{z}_1^n | \mathbf{x}_1^n)\}_{n=1}^\infty$, all secure rates R_s satisfying

$$R_s < \max_{\{\mathbf{X}_1^n\}_{n=1}^\infty} \left(\text{p-lim inf}_{n \rightarrow \infty} \frac{1}{n} i(\mathbf{X}_1^n; \mathbf{Y}_1^n) - \text{p-lim sup}_{n \rightarrow \infty} \frac{1}{n} i(\mathbf{X}_1^n; \mathbf{Z}_1^n) \right)^+$$

are achievable under the secrecy criterion (1) and the reliability criterion

$$\Pr(\hat{M} \neq M) < \epsilon_n \quad \text{for some suitably small } \epsilon_n \geq 0, \quad (3)$$

where \hat{M} is an estimate at Bob's decoder of the message M .

Lemma 1 can be leveraged to deduce the following achievability result for ISI-WTCs.⁶

Proposition 1. Consider an ISI-WTC with a finite input alphabet \mathcal{X} . For all positive integers ℓ and $\nu \geq \max(m_B, m_E)$, and any input distribution $p_{\mathbf{X}_{-\nu+1}^\ell}$, all secure rates R_s satisfying

$$R_s < \frac{1}{\ell + 2\nu} \left(I(\mathbf{X}_1^\ell; \mathbf{Y}_1^\ell | \mathbf{X}_{-\nu+1}^0) - I(\mathbf{X}_1^\ell; \mathbf{Z}_1^\ell | \mathbf{X}_{-\nu+1}^0) - 3\nu \cdot \log |\mathcal{X}| \right)^+$$

are achievable under the the secrecy criterion (1) and the reliability criterion (3).

Proof. See Appendix A. □

Definition 8. Consider an FS-JSWTC with an FSMS described by $\mathbf{Q} \in \mathcal{Q}(\mathcal{B})$. We define

$$R_s(\mathbf{Q}) \triangleq \left(\lim_{n \rightarrow \infty} \frac{1}{n} \left(I(\mathbf{S}_1^n; \mathbf{Y}_1^n | S_0) - I(\mathbf{S}_1^n; \mathbf{Z}_1^n | S_0) \right) \right)^+. \quad (4)$$

Corollary 1.1. Consider an FS-JSWTC with an FSMS described by $\mathbf{Q} \in \mathcal{Q}(\mathcal{B})$. All secure rates R_s satisfying $R_s < R_s(\mathbf{Q})$ are achievable under the secrecy criterion (1) and the reliability criterion (3).

⁶Note that since ISI channels are indecomposable FSMCs [18] (i.e., the effect of an initial state vanishes over time), the information rates are well defined even if the initial state is unknown.

Proof. Let ν be the memory order of the associated FS-JSWTC. It is easy to verify that $I(\mathbf{X}_1^n; \mathbf{Y}_1^n | \mathbf{X}_{-\nu+1}^0) = I(\mathbf{S}_1^n; \mathbf{Y}_1^n | S_0)$ and $I(\mathbf{X}_1^n; \mathbf{Z}_1^n | \mathbf{X}_{-\nu+1}^0) = I(\mathbf{S}_1^n; \mathbf{Z}_1^n | S_0)$. Invoking Proposition 1 and letting $n \rightarrow \infty$ proves the promised result. \square

We are now in a position to introduce the notion of constrained secrecy capacity, which is a key quantity to be studied in the subsequent parts of this paper.

Definition 9. Consider an FS-JSWTC as in Definition 5, where the FSMS described by \mathbf{Q} can vary in $\mathcal{Q}(\mathcal{B})$. The constrained secrecy capacity (or, more precisely, the $\mathcal{Q}(\mathcal{B})$ -constrained secrecy capacity) is defined as $C_{\mathcal{Q}(\mathcal{B})} \triangleq \max_{\mathbf{Q} \in \mathcal{Q}(\mathcal{B})} R_s(\mathbf{Q})$. \square

C. Secure Rate: Estimation

Throughout this section, we consider an FS-JSWTC as in Definition 5, where the FSMS is described by $\mathbf{Q} \in \mathcal{Q}(\mathcal{B})$. The secure rate $R_s(\mathbf{Q})$ can be efficiently estimated using variants of the algorithms in [34]. (We omit the details.) The main purpose of this section is to present an alternative approach for estimating $R_s(\mathbf{Q})$. Although the resulting algorithm by itself is slightly less efficient than the estimation algorithms based on [34], it utilizes the quantities that need to be calculated as part of the optimization algorithm presented in the next section. Therefore, when running the optimization algorithm, these quantities are readily available and can be used to estimate $R_s(\mathbf{Q})$.

Definition 10. Consider an FS-JSWTC with an FSMS described by $\mathbf{Q} \in \mathcal{Q}(\mathcal{B})$. We define

$$T_{ij}^{\text{B}}(\mathbf{Q}) \triangleq \lim_{n \rightarrow \infty} \int_{\mathbf{y}_1^n \in \mathcal{Y}^n} p_{\mathbf{Y}_1^n}(\mathbf{y}_1^n) \cdot \check{T}_{ij}^{\text{B}}(\mathbf{Q}, \mathbf{y}_1^n) d\mathbf{y}_1^n, \quad (5)$$

$$T_{ij}^{\text{E}}(\mathbf{Q}) \triangleq \lim_{n \rightarrow \infty} \int_{\mathbf{z}_1^n \in \mathcal{Z}^n} p_{\mathbf{Z}_1^n}(\mathbf{z}_1^n) \cdot \check{T}_{ij}^{\text{E}}(\mathbf{Q}, \mathbf{z}_1^n) d\mathbf{z}_1^n, \quad (6)$$

where

$$\check{T}_{ij}^{\text{B}}(\mathbf{Q}, \mathbf{y}_1^n) \triangleq \frac{1}{n} \sum_{t=1}^n \log \left(\frac{p_{S_{t-1}, S_t | \mathbf{Y}_1^n}(i, j | \mathbf{y}_1^n)^{p_{S_{t-1}, S_t | \mathbf{Y}_1^n}(i, j | \mathbf{y}_1^n) / \mu_i p_{ij}}}{p_{S_{t-1} | \mathbf{Y}_1^n}(i | \mathbf{y}_1^n)^{p_{S_{t-1} | \mathbf{Y}_1^n}(i | \mathbf{y}_1^n) / \mu_i}} \right), \quad (7)$$

$$\check{T}_{ij}^{\text{E}}(\mathbf{Q}, \mathbf{z}_1^n) \triangleq \frac{1}{n} \sum_{t=1}^n \log \left(\frac{p_{S_{t-1}, S_t | \mathbf{Z}_1^n}(i, j | \mathbf{z}_1^n)^{p_{S_{t-1}, S_t | \mathbf{Z}_1^n}(i, j | \mathbf{z}_1^n) / \mu_i p_{ij}}}{p_{S_{t-1} | \mathbf{Z}_1^n}(i | \mathbf{z}_1^n)^{p_{S_{t-1} | \mathbf{Z}_1^n}(i | \mathbf{z}_1^n) / \mu_i}} \right), \quad (8)$$

for every $(i, j) \in \mathcal{B}$.⁷ \square

⁷The expressions $\check{T}_{ij}^{\text{B}}$ and $\check{T}_{ij}^{\text{E}}$ are similar to the expression for $\check{T}_{ij}^{(N)}$ in [21, Lemma 70], part “second possibility.”

Proposition 2. The secure rate of the considered FS-JSWTC in Definition 8 can be expressed in terms of the $T_{ij}^B(\mathbf{Q})$ and $T_{ij}^E(\mathbf{Q})$ values as $R_s(\mathbf{Q}) = \left(\sum_{(i,j) \in \mathcal{B}} Q_{ij} \cdot (T_{ij}^B(\mathbf{Q}) - T_{ij}^E(\mathbf{Q})) \right)^+$.

Proof. See Appendix B. □

Remark 3. The reformulation of the secure rate in Proposition 2 can be used to efficiently estimate $R_s(\mathbf{Q})$ as shown in Algorithm 1.⁸ □

Algorithm 1 Secure Rate Estimation

Input: FSMS distribution \mathbf{Q}

- 1: Generate a sequence $\check{\mathbf{x}}_1^n$ based on the FSMS \mathbf{Q} ;
 - 2: Simulate Bob's (Eve's) channel with $\check{\mathbf{x}}_1^n$ at the input to obtain $\check{\mathbf{y}}_1^n$ ($\check{\mathbf{z}}_1^n$) at the output;
 - 3: Calculate $\check{T}_{ij}^B(\mathbf{Q}, \check{\mathbf{y}}_1^n)$ and $\check{T}_{ij}^E(\mathbf{Q}, \check{\mathbf{z}}_1^n)$ using (7) and (8), respectively, with the help of variants of the sum-product / BCJR algorithm [21];
 - 4: $\check{R}_s(\mathbf{Q}) \leftarrow \left(\sum_{(i,j) \in \mathcal{B}} Q_{ij} \cdot (\check{T}_{ij}^B(\mathbf{Q}, \check{\mathbf{y}}_1^n) - \check{T}_{ij}^E(\mathbf{Q}, \check{\mathbf{z}}_1^n)) \right)^+$;
 - 5: **return** $R_s(\mathbf{Q})$
-

IV. SECURE RATE: OPTIMIZATION

Recall the definition of the secure rate function $R_s(\mathbf{Q})$ in (4) and of the constrained secrecy capacity $C_{\mathcal{Q}(\mathcal{B})}$ in Definition 9. It appears that there is no closed-form expression for $R_s(\mathbf{Q})$ in terms of \mathbf{Q} and that the best one can do is to estimate $R_s(\mathbf{Q})$ through Monte-Carlo methods (e.g., Algorithm 1 or variants of the algorithms in [34]). Also, according to numerical investigations, the function $R_s(\mathbf{Q})$ is a fluctuating, non-concave function. Given these difficulties, the optimization problem in the specification of $C_{\mathcal{Q}(\mathcal{B})} \triangleq \max_{\mathbf{Q} \in \mathcal{Q}(\mathcal{B})} R_s(\mathbf{Q})$ in Definition 9 appears to be intractable in general. Therefore, in this section, we focus on efficient algorithms for finding a local maximum of $R_s(\mathbf{Q})$. Toward this goal, we will formulate an iterative optimization method that operates as follows.

- Assume that at the current iteration the algorithm has found the FSMS described by

$$\tilde{\mathbf{Q}} \triangleq \left\{ \tilde{Q}_{ij} \right\}_{(i,j) \in \mathcal{B}}.$$

- Around $\mathbf{Q} = \tilde{\mathbf{Q}}$, we approximate the function $R_s(\mathbf{Q})$ over $\mathcal{Q}(\mathcal{B})$ by the surrogate function $\psi_{\tilde{\mathbf{Q}}}(\mathbf{Q})$ over $\mathcal{Q}(\mathcal{B})$ satisfying the following properties:

⁸The accuracy of the approximation can be controlled by choosing n suitably large.

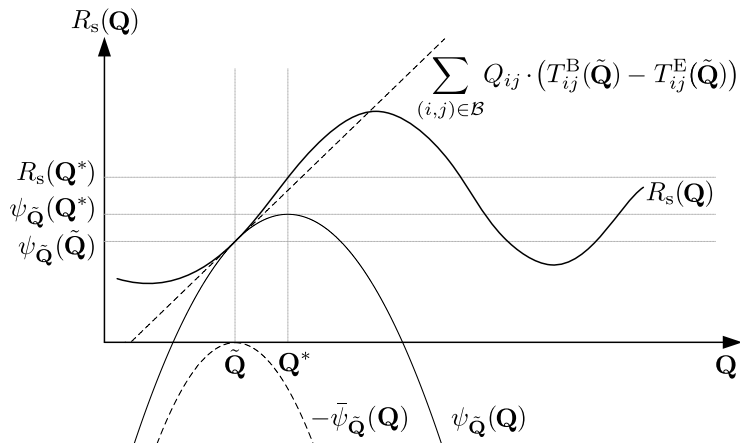


Fig. 3: Sketch of the functions appearing in the optimization algorithm discussed in Section IV. Note that, while the domain is one-dimensional in this sketch, it is multi-dimensional in the actual optimization problem.

- The value of $\psi_{\tilde{Q}}(Q)$ matches the value of $R_s(Q)$ at $Q = \tilde{Q}$.
- The gradient of $\psi_{\tilde{Q}}(Q)$ w.r.t. Q matches the gradient of $R_s(Q)$ w.r.t. Q at $Q = \tilde{Q}$.
- The function $\psi_{\tilde{Q}}(Q)$ is concave in terms of Q and can be efficiently maximized.
- Replace \tilde{Q} by the Q maximizing $\psi_{\tilde{Q}}(Q)$.

As sketched in Fig. 3, a well-defined concave surrogate function with the mentioned properties enables us to search throughout the polytope $\mathcal{Q}(\mathcal{B})$ and find the local maximum of $R_s(Q)$ over $\mathcal{Q}(\mathcal{B})$, iteratively. Similar techniques have also been proposed in [21], [44].

A. The Surrogate Function

In this section, we first introduce the surrogate function. Then, we show that the employed surrogate function fulfills the promised properties.

In the following, in the same way that we derived $\{p_{ij}\}_{(i,j) \in \mathcal{B}}$ and $\{\mu_i\}_{i \in \mathcal{S}}$ from $Q = \{Q_{ij}\}_{(i,j) \in \mathcal{B}}$, we will derive $\{\tilde{p}_{ij}\}_{(i,j) \in \mathcal{B}}$ and $\{\tilde{\mu}_i\}_{i \in \mathcal{S}}$ from $\tilde{Q} = \{\tilde{Q}_{ij}\}_{(i,j) \in \mathcal{B}}$. For every $(i, j) \in \mathcal{B}$, let $(\delta Q)_{ij} \triangleq \frac{Q_{ij} - \tilde{Q}_{ij}}{\tilde{Q}_{ij}}$ and $(\delta \mu)_i \triangleq \frac{\mu_i - \tilde{\mu}_i}{\tilde{\mu}_i}$. Moreover, let

$$\bar{\psi}_{\tilde{Q}}(Q) \triangleq \kappa' \cdot \left(\sum_{(i,j) \in \mathcal{B}} \tilde{Q}_{ij} \cdot (1 + \kappa \cdot (\delta Q)_{ij}) \cdot \log(1 + \kappa \cdot (\delta Q)_{ij}) - \sum_{i \in \mathcal{S}} \tilde{\mu}_i \cdot (1 + \kappa \cdot (\delta \mu)_i) \cdot \log(1 + \kappa \cdot (\delta \mu)_i) \right),$$

where the real parameters $0 < \kappa \leq 1$ and $\kappa' > 0$ are used to control the shape of $\bar{\psi}_{\tilde{Q}}(Q)$. For

a given operating point $\tilde{\mathbf{Q}} \in \mathcal{Q}(\mathcal{B})$, the surrogate function is specified by (see also Fig. 3)

$$\psi_{\tilde{\mathbf{Q}}}(\mathbf{Q}) \triangleq \underbrace{\sum_{(i,j) \in \mathcal{B}} Q_{ij} \cdot (T_{ij}^{\mathbf{B}}(\tilde{\mathbf{Q}}) - T_{ij}^{\mathbf{E}}(\tilde{\mathbf{Q}}))}_{\textcircled{1}} - \underbrace{\bar{\psi}_{\tilde{\mathbf{Q}}}(\mathbf{Q})}_{\textcircled{2}}. \quad (9)$$

Note that, for a fixed $\tilde{\mathbf{Q}}$, the expression $\textcircled{1}$ is linear in \mathbf{Q} , while the expression $\textcircled{2}$ is concave in \mathbf{Q} and has a zero gradient for $\mathbf{Q} = \tilde{\mathbf{Q}}$. The role of the expression $\textcircled{1}$ is to be a first-order approximation of $R_s(\mathbf{Q})$ at $\mathbf{Q} = \tilde{\mathbf{Q}}$, while the role of $\textcircled{2}$ is to regularize $\psi_{\tilde{\mathbf{Q}}}(\mathbf{Q})$. While many other expressions than $\textcircled{2}$ could have been chosen as a regularization term, the expression in $\textcircled{2}$ yields the following desirable features for $\psi_{\tilde{\mathbf{Q}}}(\mathbf{Q})$: first, the function $\psi_{\tilde{\mathbf{Q}}}(\mathbf{Q})$ can be efficiently maximized over \mathbf{Q} , second, maximizing $\psi_{\tilde{\mathbf{Q}}}(\mathbf{Q})$ implicitly also improves the entropy rate of the FSMS described by \mathbf{Q} .⁹

In the following, we examine the promised properties of the employed surrogate function (9). For brevity, we use the short-hand notations $R_s(\theta)$, $\psi_{\tilde{\mathbf{Q}}}(\theta)$, and $\tilde{\mathbf{Q}}$ for $R_s(\mathbf{Q}(\theta))$, $\psi_{\tilde{\mathbf{Q}}}(\mathbf{Q}(\theta))$, and $\mathbf{Q}(\tilde{\theta}) \in \mathcal{Q}(\mathcal{B})$, respectively.

Lemma 2 (Property 1 of the surrogate function ψ). The value of $\psi_{\tilde{\mathbf{Q}}}(\mathbf{Q})$ matches the value of $R_s(\mathbf{Q})$ at $\mathbf{Q} = \tilde{\mathbf{Q}}$, i.e., $\psi_{\tilde{\mathbf{Q}}}(\tilde{\mathbf{Q}}) = R_s(\tilde{\mathbf{Q}})$, and, in terms of the parameterization defined above, $\psi_{\tilde{\mathbf{Q}}}(\tilde{\theta}) = R_s(\tilde{\theta})$.

Proof. We start by noting that $\mathbf{Q} = \tilde{\mathbf{Q}}$ implies $(\delta Q)_{ij} = 0$ and $(\delta \mu)_i = 0$ for all $(i, j) \in \mathcal{B}$, which in turn implies that $\bar{\psi}_{\tilde{\mathbf{Q}}}(\tilde{\mathbf{Q}}) = 0$. The result $\psi_{\tilde{\mathbf{Q}}}(\tilde{\mathbf{Q}}) = R_s(\tilde{\mathbf{Q}})$ follows then from (9) along with Proposition 2. \square

Lemma 3 (Property 2 of the surrogate function ψ). The gradient of $\psi_{\tilde{\mathbf{Q}}}(\mathbf{Q})$ w.r.t. \mathbf{Q} matches the gradient of $R_s(\mathbf{Q})$ w.r.t. \mathbf{Q} at $\mathbf{Q} = \tilde{\mathbf{Q}}$, i.e., $\left. \frac{d}{d\theta} \psi_{\tilde{\mathbf{Q}}}(\theta) \right|_{\theta=\tilde{\theta}} = \left. \frac{d}{d\theta} R_s(\theta) \right|_{\theta=\tilde{\theta}}$ for any parameterization as defined above.

Proof. We start by showing that $\left. \frac{d}{d\theta} \bar{\psi}_{\tilde{\mathbf{Q}}}(\theta) \right|_{\theta=\tilde{\theta}} = 0$. Indeed,

$$\left. \frac{d}{d\theta} \bar{\psi}_{\tilde{\mathbf{Q}}}(\theta) \right|_{\theta=\tilde{\theta}} = \kappa \kappa' \cdot \left(\sum_{(i,j) \in \mathcal{B}} Q_{ij}^{\tilde{\theta}} \cdot \log(1 + \kappa \cdot (\delta Q(\tilde{\theta}))_{ij}) - \sum_{i \in \mathcal{S}} \mu_i^{\tilde{\theta}} \cdot \log(1 + \kappa \cdot (\delta \mu(\tilde{\theta}))_i) \right) \Big|_{\theta=\tilde{\theta}} = 0. \quad (10)$$

⁹Let us make the latter statement more precise for $\kappa = 1$ and $\kappa' = 1$. Namely, after some algebraic manipulations, one obtains $-\bar{\psi}_{\tilde{\mathbf{Q}}}(\mathbf{Q}) = -\sum_{(i,j) \in \mathcal{B}} Q_{ij} \cdot \log(p_{ij}) + \sum_{(i,j) \in \mathcal{B}} Q_{ij} \cdot \log(\tilde{p}_{ij})$. Note that here the first term equals the entropy rate of an FSMS satisfying the assumptions in Remark 1, whereas the latter term, which is linear in \mathbf{Q} , guarantees a zero gradient of $-\bar{\psi}_{\tilde{\mathbf{Q}}}(\mathbf{Q})$ for $\mathbf{Q} = \tilde{\mathbf{Q}}$.

We then have

$$\begin{aligned} \left. \frac{d}{d\theta} \psi_{\tilde{\mathbf{Q}}}(\theta) \right|_{\theta=\tilde{\theta}} &= \left. \frac{d}{d\theta} (\psi_{\tilde{\mathbf{Q}}}(\theta) + \bar{\psi}_{\tilde{\mathbf{Q}}}(\theta)) \right|_{\theta=\tilde{\theta}} = \left. \frac{d}{d\theta} \left(\sum_{(i,j) \in \mathcal{B}} Q_{ij}(\theta) \cdot (T_{ij}^{\text{B}}(\tilde{\theta}) - T_{ij}^{\text{E}}(\tilde{\theta})) \right) \right|_{\theta=\tilde{\theta}} \\ &= \left. \frac{d}{d\theta} \left(\sum_{(i,j) \in \mathcal{B}} Q_{ij}(\theta) \cdot (T_{ij}^{\text{B}}(\theta) - T_{ij}^{\text{E}}(\theta)) \right) \right|_{\theta=\tilde{\theta}} = \left. \frac{d}{d\theta} R_{\text{s}}(\theta) \right|_{\theta=\tilde{\theta}}, \end{aligned} \quad (11)$$

where the first equality follows from (10), the second equality follows from (9), the third equality follows from [21, Lemma 64], and the fourth equality follows from Proposition 2. \square

Remark 4. Despite the close similarity between the third and the fourth expressions in (11), this is a non-trivial result because of the non-triviality of [21, Lemma 64]. \square

Lemma 4 (Convexity of the function $\bar{\psi}_{\tilde{\mathbf{Q}}}$). The function $\bar{\psi}_{\tilde{\mathbf{Q}}}(\mathbf{Q})$ is convex over $\mathbf{Q} \in \mathcal{Q}(\mathcal{B})$.

Proof. See Appendix C. \square

Lemma 5 (Property 3 of the surrogate function ψ). The surrogate function $\psi_{\tilde{\mathbf{Q}}}(\mathbf{Q})$ is concave over $\mathbf{Q} \in \mathcal{Q}(\mathcal{B})$.

Proof. This follows immediately from Lemma 4 and from $\sum_{(i,j) \in \mathcal{B}} Q_{ij} \cdot (T_{ij}^{\text{B}}(\tilde{\mathbf{Q}}) - T_{ij}^{\text{E}}(\tilde{\mathbf{Q}}))$ being a linear function of \mathbf{Q} . \square

B. Maximizing the Surrogate Function

Let $\tilde{\mathbf{Q}} \in \mathcal{Q}(\mathcal{B})$ denote the FSMS distribution attained at the current iteration of the proposed algorithm. In the next iteration, $\tilde{\mathbf{Q}}$ is replaced by $\mathbf{Q}^* = \{Q_{ij}^*\}_{(i,j) \in \mathcal{B}}$, where

$$\mathbf{Q}^* \triangleq \arg \max_{\mathbf{Q} \in \mathcal{Q}(\mathcal{B})} \psi_{\tilde{\mathbf{Q}}}(\mathbf{Q}). \quad (12)$$

Proposition 3 (The optimum distribution \mathbf{Q}^).* The optimum FSMS distribution \mathbf{Q}^* in (12) can be calculated as follows. Let $\mathbf{A} \triangleq (A_{ij})_{i,j \in \mathcal{S}}$ be the matrix with entries

$$A_{ij} \triangleq \begin{cases} \tilde{p}_{ij} \cdot \exp\left(\frac{\tilde{T}_{ij}^{\text{B}} - \tilde{T}_{ij}^{\text{E}}}{\kappa \kappa'}\right) & ((i,j) \in \mathcal{B}) \\ 0 & (\text{otherwise}) \end{cases}, \quad (13)$$

where $\tilde{T}_{ij}^{\text{B}} \triangleq T_{ij}^{\text{B}}(\tilde{\mathbf{Q}})$ and $\tilde{T}_{ij}^{\text{E}} \triangleq T_{ij}^{\text{E}}(\tilde{\mathbf{Q}})$ are defined according to Definition 10. Note that \mathbf{A} is a non-negative matrix, i.e., a matrix with non-negative entries. Let ρ be the Perron–Frobenius eigenvalue of the matrix \mathbf{A} , with the corresponding right eigenvector $\boldsymbol{\gamma} = (\gamma_j)_{j \in \mathcal{S}}$.¹⁰ Define

$$\hat{p}_{ij}^* \triangleq \frac{A_{ij}}{\rho} \cdot \frac{\gamma_j}{\gamma_i}, \quad (i, j) \in \mathcal{B}. \quad (14)$$

Calculate $\{\hat{Q}_{ij}^*\}_{(i,j) \in \mathcal{B}}$ from $\{\hat{p}_{ij}^*\}_{(i,j) \in \mathcal{B}}$ (in the same way that we derived $\{Q_{ij}\}_{(i,j) \in \mathcal{B}}$ from $\{p_{ij}\}_{(i,j) \in \mathcal{B}}$). If

$$\kappa \geq \frac{\tilde{Q}_{ij} - \hat{Q}_{ij}^*}{\tilde{Q}_{ij}}, \quad (i, j) \in \mathcal{B}, \quad (15)$$

then the FSMS \mathbf{Q}^* is given by solving the following linear equations in terms of $\{Q_{ij}^*\}_{(i,j) \in \mathcal{B}}$

$$\left\{ \begin{array}{l} Q_{ij}^* - \hat{p}_{ij}^* \cdot \sum_{j' \in \vec{\mathcal{S}}_i} Q_{ij'}^* - \frac{1-\kappa}{\kappa} \cdot (\tilde{\mu}_i \hat{p}_{ij}^* - \tilde{Q}_{ij}) = 0, \quad (i, j) \in \mathcal{B}, \\ \sum_{r \in \overleftarrow{\mathcal{S}}_i} Q_{ri}^* - \sum_{j \in \vec{\mathcal{S}}_i} Q_{ij}^* = 0, \quad i \in \mathcal{S}, \\ \sum_{(i,j) \in \mathcal{B}} Q_{ij}^* = 1, \end{array} \right.$$

Proof. See Appendix D. □

Remark 5. Proposition 3 applies Perron–Frobenius theory for irreducible non-negative matrices. One can verify that the matrix \mathbf{A} is irreducible except for uninteresting boundary cases. □

Remark 6. Increasing the real parameters κ and κ' makes the surrogate function to be narrower and steeper, which reduces the aggressiveness of the searching step size. □

Procedure 1. In the following, Algorithm 1 is leveraged to efficiently find an approximation $\check{\mathbf{Q}}^*$ to \mathbf{Q}^* by using the procedure in Proposition 3.¹¹

- 1) Generate a sequence $\check{\mathbf{x}}_1^n$ based on the FSMS $\mathbf{Q} = \tilde{\mathbf{Q}}$.
- 2) Simulate Bob's (Eve's) channel with $\check{\mathbf{x}}_1^n$ at the input to obtain $\check{\mathbf{y}}_1^n$ ($\check{\mathbf{z}}_1^n$) at the output.
- 3) For every $(i, j) \in \mathcal{B}$, compute $\check{T}_{ij}^{\text{B}}(\tilde{\mathbf{Q}}, \check{\mathbf{y}}_1^n)$ and $\check{T}_{ij}^{\text{E}}(\tilde{\mathbf{Q}}, \check{\mathbf{z}}_1^n)$ according to (7) and (8).

¹⁰Recall that the Perron–Frobenius eigenvalue of an irreducible non-negative matrix is the eigenvalue with the largest absolute value. One can show that the Perron–Frobenius eigenvalue is a positive real number and that the corresponding right eigenvector can be multiplied by a suitable scalar such that all entries are positive real numbers.

¹¹The accuracy of the approximation can be controlled by choosing n suitably large.

4) Let $\check{\mathbf{A}} \triangleq (\check{A}_{ij})_{i,j \in \mathcal{S}}$ be the matrix with entries

$$\check{A}_{ij} \triangleq \begin{cases} \check{p}_{ij} \cdot \exp\left(\frac{\check{T}_{ij}^{\text{B}}(\tilde{\mathbf{Q}}, \check{\mathbf{y}}_1^n) - \check{T}_{ij}^{\text{E}}(\tilde{\mathbf{Q}}, \check{\mathbf{z}}_1^n)}{\kappa \kappa'}\right) & ((i, j) \in \mathcal{B}) \\ 0 & (\text{otherwise}) \end{cases}$$

5) Find the Perron–Frobenius eigenvalue $\check{\rho}$ and the corresponding right eigenvector $\check{\boldsymbol{\gamma}}$ of the matrix $\check{\mathbf{A}}$.

6) Compute $\check{p}_{ij}^* \triangleq \frac{\check{A}_{ij}}{\check{\rho}} \cdot \frac{\check{\gamma}_j}{\check{\gamma}_i}$, for all $(i, j) \in \mathcal{B}$. Then, calculate $\{\check{Q}_{ij}^*\}_{(i,j) \in \mathcal{B}}$ from $\{\check{p}_{ij}^*\}_{(i,j) \in \mathcal{B}}$ (in the same way that we derived $\{Q_{ij}\}_{(i,j) \in \mathcal{B}}$ from $\{p_{ij}\}_{(i,j) \in \mathcal{B}}$).

7) If $\kappa \geq (\tilde{Q}_{ij} - \check{Q}_{ij}^*)/\tilde{Q}_{ij}$, for all $(i, j) \in \mathcal{B}$, then the FSMS $\check{\mathbf{Q}}^*$ is given by solving the following system of linear equations in terms of $\{\check{Q}_{ij}^*\}_{(i,j) \in \mathcal{B}}$.

$$\begin{cases} \check{Q}_{ij}^* - \check{p}_{ij}^* \sum_{j' \in \vec{\mathcal{S}}_i} \check{Q}_{ij'}^* - \frac{1-\kappa}{\kappa} \cdot (\tilde{\mu}_i \check{p}_{ij}^* - \tilde{Q}_{ij}) = 0, & (i, j) \in \mathcal{B}, \\ \sum_{r \in \overleftarrow{\mathcal{S}}_i} \check{Q}_{ri}^* - \sum_{j \in \vec{\mathcal{S}}_i} \check{Q}_{ij}^* = 0, & i \in \mathcal{S}, \\ \sum_{(i,j) \in \mathcal{B}} \check{Q}_{ij}^* = 1. \end{cases} \quad (16)$$

8) Else, if $\kappa < (\tilde{Q}_{ij} - \check{Q}_{ij}^*)/\tilde{Q}_{ij}$, for any $(i, j) \in \mathcal{B}$, suitably change κ and go to Step 4.

Remark 7 (The EM Viewpoint). Procedure 1 can be considered as a variation of the well-known EM algorithm [45] comprised of two steps: Expectation (E-step) and Maximization (M-step). Namely, identifying a concave surrogate function around a local operating point resembles the E-step and maximization of the surrogate function to achieve a higher secure rate corresponds to the M-step. Given this, Algorithm 2 has a similar convergence behavior as the EM algorithm [46] (as outlined in Remark 8). \square

Algorithm 2 summarizes the complete procedure of the proposed optimization method.

Remark 8 (Convergence). A similar manipulation as performed in [21, Eqs. (52), (53)] shows that $\psi_{\check{\mathbf{Q}}}(\mathbf{Q}^*) \geq \psi_{\check{\mathbf{Q}}}(\mathbf{Q})$, for all $\mathbf{Q} \in \mathcal{Q}(\mathcal{B})$. Consequently, at each iteration r , we have $\psi_{\mathbf{Q}^{(r)}}(\mathbf{Q}^{(r+1)}) \geq \psi_{\mathbf{Q}^{(r)}}(\mathbf{Q}^{(r)})$, where the equality $\psi_{\mathbf{Q}^{(r)}}(\mathbf{Q}^{(r+1)}) = \psi_{\mathbf{Q}^{(r)}}(\mathbf{Q}^{(r)})$ occurs at the stationary point of Algorithm 2. The stationary points of the algorithm correspond to the critical points (i.e., local maxima, local minima, and saddle points) of $R_s(\mathbf{Q})$ over the polytope $\mathcal{Q}(\mathcal{B})$. Since the local minima and the saddle points are not stable stationary points

Algorithm 2 Secure Rate Optimization

- 1: set $r \leftarrow 0$;
 - ▷ *Iteration* (until convergence)
 - 2: Apply Procedure 1 with input $\mathbf{Q} = \mathbf{Q}^{(r)}$ and output $\check{\mathbf{Q}}^*$
 - 3: $r \leftarrow r + 1$;
 - 4: $\mathbf{Q}^{(r)} \leftarrow \check{\mathbf{Q}}^*$;
 - ◁ *End*
 - 5: Use Algorithm 1 with input $\mathbf{Q} = \mathbf{Q}^{(r)}$ and output \check{R}_s ;
 - 6: **return** \check{R}_s .
-

of Algorithm 2, the algorithm converges to a local maximum of $R_s(\mathbf{Q})$ achievable from a starting point $\mathbf{Q}^{(0)} \in \mathcal{Q}(\mathcal{B})$. \square

Remark 9 (Complexity). The complexity of one iteration of Algorithm 2 is $\mathcal{O}(n \cdot 2^\nu + (2^\nu)^3)$, where the first term stems from estimating $\check{T}_{ij}^B(\mathbf{Q}, \check{\mathbf{y}}_1^n)$ and $\check{T}_{ij}^E(\mathbf{Q}, \check{\mathbf{z}}_1^n)$, along with the Perron-Frobenius eigenvalue $\check{\rho}$, and where the second term stems from solving the system of linear equations in (16). (Potentially, the sparsity of the system of linear equations in (16) can be used to reduce the latter complexity estimate.) \square

V. PRACTICAL IMPLICATIONS AND SIMULATION RESULTS

In this section, we first approximate an NB-IoT uplink channel in a challenging environment by an ISI channel as in Definition 3. Afterwards, we describe two practically relevant wiretapping scenarios and study the maximum achievable secure rates by applying Algorithm 2 to the resulting ISI-WTCs. Note that in the following, the variable $t_c \in \mathbb{R}$ will be used to denote continuous time, in order to distinguish it from the discrete time variable $t \in \mathbb{Z}$ that is used elsewhere in this paper.

A. NB-IoT Uplink Channel

Let $X(t_c)$, $Y(t_c)$, and $N(t_c)$ be continuous-time random signals corresponding to, respectively, the channel's input, the channel's output, and additive noise. The general model for the multipath channel, consisting of a direct path and $m_c \in \mathbb{Z}$ tapped-delay paths, is described by $Y(t_c) \triangleq \sum_{\ell=0}^{m_c} |g_{c,\ell}| e^{i\theta_\ell} \cdot X(t_c - \tau_\ell) + N(t_c)$, where i denotes the imaginary unit and where the real parameters $|g_{c,\ell}|$, θ_ℓ , and τ_ℓ are the gain, the phase rotation, and the

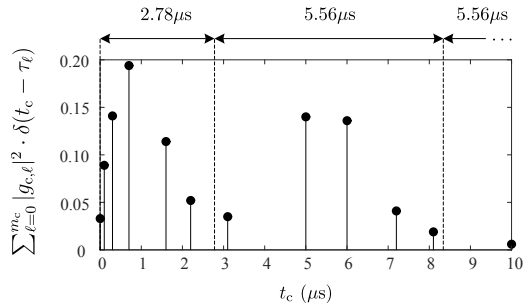


Fig. 4: Power-delay profile of the multipath channel.

TABLE I:
ISI CHANNEL MODEL CORRESPONDING TO
THE POWER-DELAY PROFILE OF FIG. 4,
WITH $W_{\text{PRB}}^{-1} = 5.56 \mu\text{s}$, $f_{\text{carr}} = 900 \text{ MHz}$.

ℓ	Period (μs)	$ g_\ell ^2$	$e^{-i2\pi f_{\text{carr}}\tau_\ell}$
0	0 – 2.78	0.624	1
1	2.78 – 8.33	0.370	1
2	8.33 – 13.89	0.006	1

delay introduced by the ℓ -th path, respectively.¹² Fig. 4 illustrates a typical power-delay profile of a multipath channel that was measured in an urban area with moderate to high tree density [47, Fig. 2.51].

The uplink channel of the NB-IoT occupies a single physical resource block (PRB) from the LTE configuration, and so the bandwidth of the transmitted signal is restricted to $W_{\text{PRB}} = 180 \text{ kHz}$ [9, Sec. 5.2.3]. As can be seen from Fig. 4, the delay spread of the wireless channel exceeds the duration of a single channel use ($W_{\text{PRB}}^{-1} = 5.56 \mu\text{s}$).¹³ This issue along with the multipath propagation gives rise to ISI. As shown in Table I, the ISI tap coefficients are captured by sampling at times $\frac{W_{\text{PRB}}^{-1}}{2} + \ell \cdot W_{\text{PRB}}^{-1}$ for $\ell \in \{0, 1, 2\}$. By ignoring the third tap, which can be justified due to its relative amplitude being 10dB below the first tap, the sampled output of a filter matched to the shaping pulse at the receiver becomes $g(D) = 0.792 + 0.610D$.

Before introducing the wiretapping scenario, we consider a point-to-point setup where the only channel input constraint is an average-energy constraint. This allows us to use the well-known “water-pouring” formulas for analyzing capacities of Bob’s and Eve’s point-to-point channels in the examined ISI-WTC. Let us consider the average-energy constraint per input symbol E_s (in Joules), the symbol duration T (in seconds), a perfect lowpass filter of bandwidth $W \triangleq \frac{1}{2T}$ with the sampling at Nyquist frequency $1/T$ at the receiver, and the power spectral density $N(f)$ (in Watts per Hertz) of the additive Gaussian noise before the

¹²We assume that the local oscillators at the transmitter and the receiver terminals are synchronous, and so the phase reference θ_0 is known. Then, for $\theta_0 = 0$ and $\tau_0 = 0$, the phase rotation in the ℓ -th path (w.r.t. the direct path) is given by $\theta_\ell = -2\pi f_{\text{carr}}\tau_\ell$, where f_{carr} is the carrier frequency.

¹³The statistical channel models in COST 207 are valid for applications having an average bandwidth of about 200 kHz [47, Sec. 2.5.4.2].

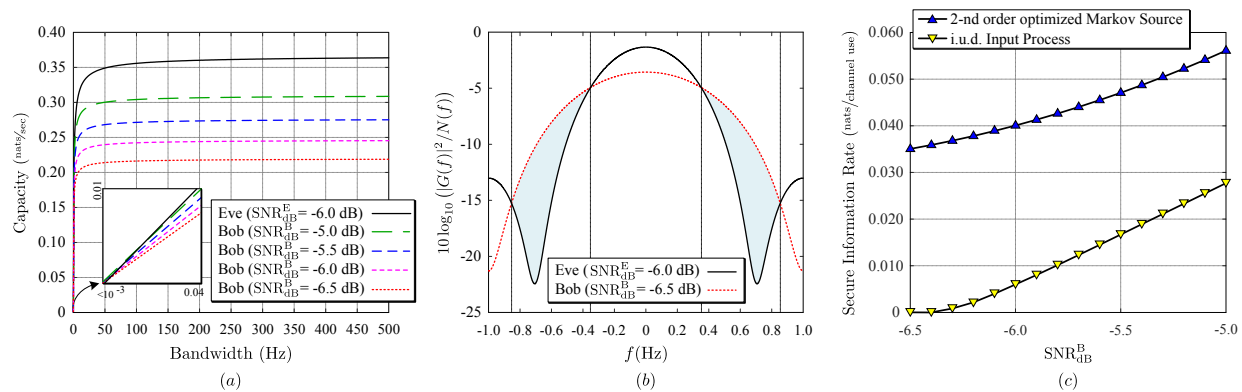


Fig. 5: Example 2 ($g^B(D) = 0.792 + 0.610D$, $g^E(D) = 0.446 + 0.633D + 0.633D^2$, $\text{SNR}_{\text{dB}}^E = -6.0$ dB). (a): Unconstrained capacities of Bob's and Eve's point-to-point channels in nats/sec with normalized average-energy constraint $E_s = 1$ J. (b): Gain-to-noise power spectrum ratios of Bob's and Eve's point-to-point channels in dB/Hz. (c): Secure information rates achieved by various input processes in nats/channel use.

lowpass filter. The unconstrained (besides some average-energy constraint) capacity of an ISI channel, described by $(g(D) = \sum_{t=0}^m g_t D^t, N(f))$, is given by the “water-pouring” formula (see, e.g., [48]) $C(g, W) = \frac{1}{2} \cdot \int_{-\infty}^{\infty} \log^+ \left(\frac{\alpha}{N(f)/|G(f)|^2} \right) df$ where $G(f) = \frac{\sum_{\ell=0}^m g_\ell e^{-i2\ell\pi fT}}{\sqrt{\sum_{\ell=0}^m |g_\ell|^2}}$ if $|f| \leq W$ and $G(f) = 0$ otherwise, and where $\alpha > 0$ is chosen such that $E_s = \int_{-\infty}^{\infty} \left(\alpha - \frac{N(f)}{|G(f)|^2} \right)^+ df$.

B. Wiretapping Scenarios and Achievable Secure Rates

In the following two examples, we apply Algorithm 2 for optimizing the parameters of an FSMS characterized by $(\mathcal{X} = \{+\sqrt{E_s}, -\sqrt{E_s}\}, \bar{\nu} \triangleq 2, p_{X_t|X_{t-\bar{\nu}}^{t-1}}(x_t|\mathbf{x}_{t-\bar{\nu}}^{t-1}))$, at the input of two different ISI-WTCs.¹⁴ We consider a setup where Bob's channel and Eve's channel have normalized transfer polynomials¹⁵ $g^B(D)$ and $g^E(D)$, and additive white Gaussian noise of variance σ_B^2 and σ_E^2 , respectively. Accordingly, the signal-to-noise ratios (SNRs) of Bob's channel and Eve's channel are defined as, respectively, $\text{SNR}^B \triangleq E_s/\sigma_B^2$ and $\text{SNR}^E \triangleq E_s/\sigma_E^2$.¹⁶

Example 2. In the first scenario, Bob's channel is assumed to be the ISI channel derived from Table I, i.e., $g^B(D) = 0.792 + 0.610D$. Also, Eve's channel is assumed to be another ISI channel with the same delay profile as in Table I, but with different tap coefficients. Since it is challenging for Eve to intercept the transmitted signals from the line-of-sight transmission,

¹⁴The BPSK modulation is proposed for the narrowband physical uplink shared channel (NPUSCH), both for data (NPUSCH Format 1) and control (NPUSCH Format 2) channels [9, Tab. 10.1.3.2-1].

¹⁵A normalized transfer polynomial $g(D) \triangleq \sum_{t=0}^m g_t D^t \in \mathbb{C}[D]$ has to satisfy $\sum_{t=0}^m |g_t|^2 = 1$. (See, e.g., [48].)

¹⁶If desired, these SNR values can be re-expressed in terms of E_s/N_0 values, where $N_0/2$ is the two-sided power spectral density of the AWGN process: $E_s/N_0 = \frac{1}{2} \cdot (E_s/\sigma^2)$.

the relative amplitude of Eve’s direct path is assumed to be (at least) 2.5 dB below Bob’s direct path. However, the other tap coefficients are then assumed to be such that Eve’s channel has the highest unconstrained capacity among all ISI channels satisfying the delay profile of Table I, i.e., $(g_t^E)_{t=0}^2 = \arg \max_{\tilde{g}^E: |\tilde{g}_0^E| \leq |g_0^B| - 2.5\text{dB}} C(\tilde{g}^E, W)$. Solving this problem for $g_0^B = 0.792$ leads to $g^E(D) = 0.446 + 0.633D + 0.633D^2$. The resulting unconstrained capacities of Bob’s and Eve’s point-to-point channels are depicted in Fig. 5(a).¹⁷ It can be seen from Fig. 5(a) that Eve’s channel has a higher unconstrained capacity than Bob’s channel for sufficiently large enough bandwidth. In this sense, Bob’s channel is “worse” than Eve’s channel. However, luckily for Bob, there are frequencies where Bob’s channel has a better gain-to-noise power spectrum ratio than Eve’s channel, as can be seen from Fig. 5(b). These spectral discrepancies can be exploited by a suitably tuned input source toward obtaining positive secure rates.

Fig. 5(c) shows the obtained secure rates: on the one hand for an *unoptimized* FSMS, i.e., an FSMS producing the independent and uniformly distributed (i.u.d.) symbols, and, on the other hand, for an *optimized* FSMS, where the optimization was done with the help of Algorithm 2. In this plot, the best obtained secure rate is plotted after running Algorithm 2 for 100 different initializations.¹⁸ □

In the next example, i.e., Example 3, we consider the same scenario as in Example 2, but where Bob’s channel is swapped with Eve’s channel. For comparison, note that in a wiretap channel setup with *memoryless* additive Gaussian noise channels, if the first scenario is such that positive secure rates are possible, then in the second scenario, i.e., after swapping Bob’s channel with Eve’s channel, the secure rate is zero [52].

Example 3. In the second scenario, the roles of the receiver terminals in Example 2 are swapped, i.e., $g^B(D) = 0.446 + 0.633D + 0.633D^2$ and $g^E(D) = 0.792 + 0.610D$. In this case (see Fig. 6), Bob’s channel has a higher unconstrained capacity than Eve’s channel for sufficiently large enough bandwidth. In this sense, it is not unexpected that positive secure

¹⁷Since the NB-IoT protocol promises to provide reliable connections with low power consumption, we consider low-SNR regimes both for Bob’s channel and Eve’s channel [49].

¹⁸The parameters κ and κ' in Algorithm 2 took values in the ranges $0.9 \leq \kappa \leq 1.0$ and $4 \leq \kappa' \leq 6$, respectively. Typically, 60 to 80 iterations were needed to reach numerical convergence. The initializations were generated with the help of Weyl’s $|\mathcal{S}|$ -dimensional equi-distributed sequences [50]. (Simulation files are available online [51].)

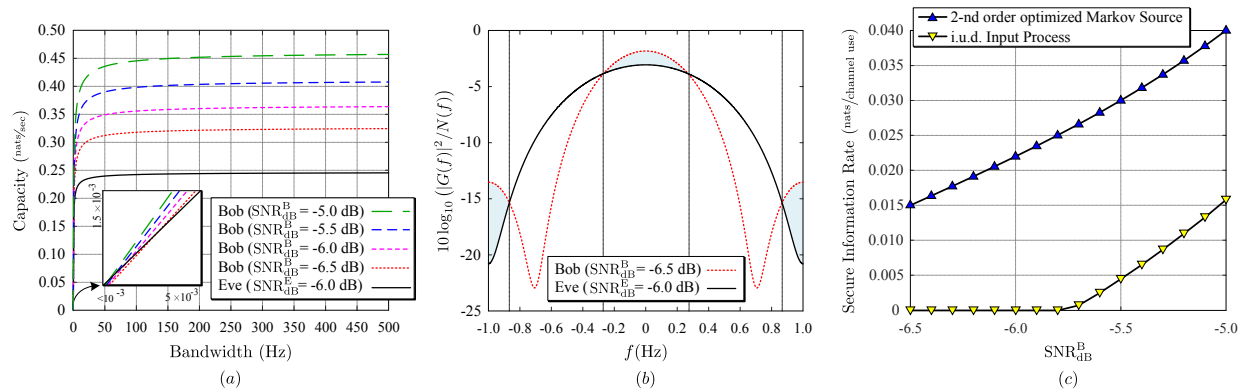


Fig. 6: Example 3 ($g^B(D) = 0.446 + 0.633D + 0.633D^2$, $g^E(D) = 0.792 + 0.610D$, $\text{SNR}_{\text{dB}}^E = -6.0$ dB). (a): Unconstrained capacities of Bob's and Eve's point-to-point channels in nats/sec with normalized average-energy constraint $E_s = 1$ J. (b): Gain-to-noise power spectrum ratios of Bob's and Eve's point-to-point channels in dB/Hz. (c): Secure information rates achieved by various input processes in nats/channel use.

rates are possible. Nevertheless, it is worthwhile to point out that here positive secure rates are possible even though Bob's channel has larger memory than Eve's channel, and for some selections of SNR_{dB}^B , higher noise power than Eve's channel. \square

C. Discussion

In a wiretap channel setup with memoryless additive Gaussian noise channels, Eve's channel necessarily has to be noisier than Bob's channel to achieve a positive secrecy capacity [52]. This results in the capacity of Eve's channel being less than the capacity of Bob's channel. The optimized FSMSs achieved positive secure rates over the ISI-WTCs, (i) even when the unconstrained capacity of Bob's channel is smaller than the unconstrained capacity of Eve's channel (as pointed out in Example 2), (ii) even when Bob's channel tolerates both a higher noise power and a larger memory compared with Eve's channel (as pointed out in Example 3). These results confirm the feasibility of benefiting from the spectral discrepancies of Bob's and Eve's point-to-point channels by using optimized FSMSs—without consuming any extra power for cooperative jamming or injecting artificial noise (as it was done in [30], [31]).

VI. CONCLUSION

In this paper, we have derived a lower bound on the achievable secure rates over ISI-WTCs. Then, we have optimized an FSMS at the input of an ISI-WTC toward (locally)

maximizing the obtained secure rates. Because directly maximizing the secure rate function is challenging, we have iteratively approximated the secure rate function by concave surrogate functions whose maximum can be found efficiently. Our numerical results show that by implicitly using the discrepancies between the frequency responses of Bob's channel and Eve's channel, it is possible to achieve positive secure rates also for setups where the unconstrained capacity of Eve's channel is larger than the unconstrained capacity of Bob's channel.

APPENDIX A

PROOF OF PROPOSITION 1

Let $\{\mathbf{X}_{k(\ell+2\nu)-\nu+1}^{k(\ell+2\nu)+(\ell+\nu)}\}_{k=-\infty}^{+\infty}$ be a block i.i.d. process where each block has length $\ell+2\nu$. It suffices to specify the distribution of a single block $\mathbf{X}_{k(\ell+2\nu)-\nu+1}^{k(\ell+2\nu)+(\ell+\nu)}$. In order to ensure that there is no interference across blocks, we set $X_{k(\ell+2\nu)+(\ell+1)} \triangleq 0, \dots, X_{k(\ell+2\nu)+(\ell+\nu)} \triangleq 0$, while allowing $\mathbf{X}_{k(\ell+2\nu)-\nu+1}^{k(\ell+2\nu)+\ell}$ to be arbitrarily distributed. Obviously, $\{\mathbf{X}_{k(\ell+2\nu)-\nu+1}^{k(\ell+2\nu)+(\ell+\nu)}, \mathbf{Y}_{k(\ell+2\nu)-\nu+1}^{k(\ell+2\nu)+(\ell+\nu)}\}_{k=-\infty}^{+\infty}$ and $\{\mathbf{X}_{k(\ell+2\nu)-\nu+1}^{k(\ell+2\nu)+(\ell+\nu)}, \mathbf{Z}_{k(\ell+2\nu)-\nu+1}^{k(\ell+2\nu)+(\ell+\nu)}\}_{k=-\infty}^{+\infty}$ are both joint block i.i.d. processes as well.

Let $\{X_t, Y_t\}_{t=1}^n = \{\mathbf{X}_{k(\ell+2\nu)-\nu+1}^{k(\ell+2\nu)+(\ell+\nu)}, \mathbf{Y}_{k(\ell+2\nu)-\nu+1}^{k(\ell+2\nu)+(\ell+\nu)}\}_{k=1}^{n'}$, where n' denotes the number of i.i.d. blocks in $\{X_t, Y_t\}_{t=1}^n$. Then,

$$\begin{aligned} \lim_{n \rightarrow \infty} \frac{1}{n} i(\mathbf{X}_1^n; \mathbf{Y}_1^n) &= \lim_{n \rightarrow \infty} \frac{n'}{n} \left(\frac{1}{n'} \sum_{k=1}^{n'} i(\mathbf{X}_{k(\ell+2\nu)-\nu+1}^{k(\ell+2\nu)+(\ell+\nu)}, \mathbf{Y}_{k(\ell+2\nu)-\nu+1}^{k(\ell+2\nu)+(\ell+\nu)}) \right) \\ &= \frac{1}{\ell+2\nu} I(\mathbf{X}_{-\nu+1}^{\ell+\nu}; \mathbf{Y}_{-\nu+1}^{\ell+\nu}), \quad \text{w.p. 1,} \end{aligned} \quad (17)$$

where the second equality follows from the strong law of large numbers and $n = n' \cdot (\ell + 2\nu)$.

With an analogous manipulation, we have

$$\lim_{n \rightarrow \infty} \frac{1}{n} i(\mathbf{X}_1^n; \mathbf{Z}_1^n) = \frac{1}{\ell+2\nu} I(\mathbf{X}_{-\nu+1}^{\ell+\nu}; \mathbf{Z}_{-\nu+1}^{\ell+\nu}), \quad \text{w.p. 1.} \quad (18)$$

Note $I(\mathbf{X}_{-\nu+1}^{\ell+\nu}; \mathbf{Y}_{-\nu+1}^{\ell+\nu}) \geq I(\mathbf{X}_{-\nu+1}^{\ell}; \mathbf{Y}_1^{\ell}) = I(\mathbf{X}_{-\nu+1}^0; \mathbf{Y}_1^{\ell}) + I(\mathbf{X}_1^{\ell}; \mathbf{Y}_1^{\ell} | \mathbf{X}_{-\nu+1}^0) \geq I(\mathbf{X}_1^{\ell}; \mathbf{Y}_1^{\ell} | \mathbf{X}_{-\nu+1}^0)$.

Moreover, $I(\mathbf{X}_{-\nu+1}^{\ell+\nu}; \mathbf{Z}_{-\nu+1}^{\ell+\nu}) = I(\mathbf{X}_{-\nu+1}^{\ell}; \mathbf{Z}_{-\nu+1}^{\ell+\nu})$

$$\begin{aligned} &= I(\mathbf{X}_{-\nu+1}^{\ell}; \mathbf{Z}_1^{\ell}) + I(\mathbf{X}_{-\nu+1}^{\ell}; \mathbf{Z}_{-\nu+1}^0 | \mathbf{Z}_1^{\ell}) + I(\mathbf{X}_{-\nu+1}^{\ell}; \mathbf{Z}_{\ell+1}^{\ell+\nu} | \mathbf{Z}_{-\nu+1}^{\ell}) \\ &= I(\mathbf{X}_1^{\ell}; \mathbf{Z}_1^{\ell} | \mathbf{X}_{-\nu+1}^0) + I(\mathbf{X}_{-\nu+1}^0; \mathbf{Z}_1^{\ell}) + I(\mathbf{X}_{-\nu+1}^{\ell}; \mathbf{Z}_{-\nu+1}^0 | \mathbf{Z}_1^{\ell}) + I(\mathbf{X}_{-\nu+1}^{\ell}; \mathbf{Z}_{\ell+1}^{\ell+\nu} | \mathbf{Z}_{-\nu+1}^{\ell}) \\ &= I(\mathbf{X}_1^{\ell}; \mathbf{Z}_1^{\ell} | \mathbf{X}_{-\nu+1}^0) + I(\mathbf{X}_{-\nu+1}^0; \mathbf{Z}_1^{\ell}) + I(\mathbf{X}_{-\nu+1}^0; \mathbf{Z}_{-\nu+1}^0 | \mathbf{Z}_1^{\ell}) + I(\mathbf{X}_{-\nu+1}^{\ell}; \mathbf{Z}_{\ell+1}^{\ell+\nu} | \mathbf{Z}_{-\nu+1}^{\ell}) \\ &\leq I(\mathbf{X}_1^{\ell}; \mathbf{Z}_1^{\ell} | \mathbf{X}_{-\nu+1}^0) + 3\nu \log |\mathcal{X}|. \end{aligned}$$

Combining Lemma 1 with (17), (18), and the above lower and upper bounds concludes the proof.

APPENDIX B

PROOF OF PROPOSITION 2

Reformulating the expression in (4), we obtain

$$\begin{aligned} R_s &= \lim_{n \rightarrow \infty} \frac{1}{n} \sum_{t=1}^n \left(I(S_t; \mathbf{Y}_1^n | \mathbf{S}_0^{t-1}) - I(S_t; \mathbf{Z}_1^n | \mathbf{S}_0^{t-1}) \right) = \lim_{n \rightarrow \infty} \frac{1}{n} \sum_{t=1}^n \left(I(S_t; \mathbf{Y}_1^n | S_{t-1}) - I(S_t; \mathbf{Z}_1^n | S_{t-1}) \right) \\ &= \lim_{n \rightarrow \infty} \frac{1}{n} \sum_{t=1}^n \left(H(S_t | \mathbf{Z}_1^n, S_{t-1}) - H(S_t | \mathbf{Y}_1^n, S_{t-1}) \right) = \sum_{(i,j) \in \mathcal{B}} Q_{ij} \cdot \left(T_{ij}^{\mathbf{B}}(\mathbf{Q}) - T_{ij}^{\mathbf{E}}(\mathbf{Q}) \right), \end{aligned}$$

where the $(\cdot)^+$ operator has been omitted for clarity of the presentation and where the last equality is based on expressing $H(S_t | \mathbf{Y}_1^n, S_{t-1})$ as

$$\begin{aligned} H(S_t | \mathbf{Y}_1^n, S_{t-1}) &= - \sum_{(i,j) \in \mathcal{B}} \int_{\mathbf{y}_1^n \in \mathcal{Y}^n} p_{S_t, S_{t-1}, \mathbf{Y}_1^n}(j, i, \mathbf{y}_1^n) \cdot \log \left(p_{S_t | S_{t-1}, \mathbf{Y}_1^n}(j | i, \mathbf{y}_1^n) \right) d\mathbf{y}_1^n \\ &= - \sum_{(i,j) \in \mathcal{B}} \int_{\mathbf{y}_1^n \in \mathcal{Y}^n} p_{S_t, S_{t-1}, \mathbf{Y}_1^n}(j, i, \mathbf{y}_1^n) \cdot \left(\log \left(\frac{p_{S_t, S_{t-1}, \mathbf{Y}_1^n}(j, i, \mathbf{y}_1^n)}{p_{\mathbf{Y}_1^n}(\mathbf{y}_1^n)} \right) - \log \left(\frac{p_{S_{t-1}, \mathbf{Y}_1^n}(i, \mathbf{y}_1^n)}{p_{\mathbf{Y}_1^n}(\mathbf{y}_1^n)} \right) \right) d\mathbf{y}_1^n \\ &= - \sum_{(i,j) \in \mathcal{B}} \mu_i p_{ij} \cdot \int_{\mathbf{y}_1^n \in \mathcal{Y}^n} \left(p_{\mathbf{Y}_1^n | S_{t-1}, S_t}(\mathbf{y}_1^n | i, j) \cdot \log \left(p_{S_{t-1}, S_t | \mathbf{Y}_1^n}(i, j | \mathbf{y}_1^n) \right) \right. \\ &\quad \left. - p_{\mathbf{Y}_1^n | S_{t-1}}(\mathbf{y}_1^n | i) \cdot \log \left(p_{S_{t-1} | \mathbf{Y}_1^n}(i | \mathbf{y}_1^n) \right) \right) d\mathbf{y}_1^n \\ &= - \sum_{(i,j) \in \mathcal{B}} \mu_i p_{ij} \cdot \int_{\mathbf{y}_1^n \in \mathcal{Y}^n} \left(\frac{p_{S_{t-1}, S_t | \mathbf{Y}_1^n}(i, j | \mathbf{y}_1^n)}{\mu_i p_{ij}} \cdot p_{\mathbf{Y}_1^n}(\mathbf{y}_1^n) \cdot \log \left(p_{S_{t-1}, S_t | \mathbf{Y}_1^n}(i, j | \mathbf{y}_1^n) \right) \right. \\ &\quad \left. - \frac{p_{S_{t-1} | \mathbf{Y}_1^n}(i | \mathbf{y}_1^n)}{\mu_i} \cdot p_{\mathbf{Y}_1^n}(\mathbf{y}_1^n) \cdot \log \left(p_{S_{t-1} | \mathbf{Y}_1^n}(i | \mathbf{y}_1^n) \right) \right) d\mathbf{y}_1^n \\ &= - \sum_{(i,j) \in \mathcal{B}} \mu_i p_{ij} \cdot \left(\int_{\mathbf{y}_1^n \in \mathcal{Y}^n} p_{\mathbf{Y}_1^n}(\mathbf{y}_1^n) \cdot \log \left(\frac{p_{S_{t-1}, S_t | \mathbf{Y}_1^n}(i, j | \mathbf{y}_1^n)^{p_{S_{t-1}, S_t | \mathbf{Y}_1^n}(i, j | \mathbf{y}_1^n) / \mu_i p_{ij}}}{p_{S_{t-1} | \mathbf{Y}_1^n}(i | \mathbf{y}_1^n)^{p_{S_{t-1} | \mathbf{Y}_1^n}(i | \mathbf{y}_1^n) / \mu_i}} \right) \right) d\mathbf{y}_1^n, \end{aligned}$$

with an analogous expression for $H(S_t | \mathbf{Z}_1^n, S_{t-1})$, along with using (5) and (6).

APPENDIX C

PROOF OF LEMMA 4

Besides the assumptions on the parameterizations $\mathbf{Q}(\theta)$ made in Remark 2, we will also assume that for all $(i, j) \in \mathcal{B}$, the functions $Q_{ij}(\theta)$ and $\mu_i(\theta)$ are affine functions in terms of θ ,

which implies $Q_{ij}^{\theta\theta}(\theta) = 0$ and $\mu_i^{\theta\theta}(\theta) = 0$, where the superscript $\theta\theta$ denotes the second-order derivative w.r.t. θ .

Denoting the second-order derivative of $\bar{\psi}_{\mathbf{Q}}(\theta)$ by $\bar{\psi}_{\mathbf{Q}}^{\theta\theta}(\theta)$, we observe that the claim in the lemma statement is equivalent to $\bar{\psi}_{\mathbf{Q}}^{\theta\theta}(\theta) \geq 0$ for all possible parameterizations of $\mathbf{Q}(\theta)$ that satisfy the above-mentioned conditions.

Some straightforward calculations show that

$$\bar{\psi}_{\mathbf{Q}}^{\theta\theta}(\theta) = \kappa^2 \kappa' \cdot \left(\sum_{(i,j) \in \mathcal{B}} \frac{(Q_{ij}^\theta)^2}{Q_{ij}} - \sum_{i \in \mathcal{S}} \frac{(\mu_i^\theta)^2}{\mu_i} \right) = \kappa^2 \kappa' \cdot \sum_{i \in \mathcal{S}} \left(\left(\sum_{j \in \vec{\mathcal{S}}_i} \frac{(Q_{ij}^\theta)^2}{Q_{ij}} \right) - \frac{(\mu_i^\theta)^2}{\mu_i} \right).$$

Noting that for any $i \in \mathcal{S}$ it holds that

$$\sum_{j \in \vec{\mathcal{S}}_i} \frac{(Q_{ij}^\theta)^2}{Q_{ij}} = \mu_i \cdot \sum_{j \in \vec{\mathcal{S}}_i} \frac{Q_{ij}}{\mu_i} \cdot \left(\frac{Q_{ij}^\theta}{Q_{ij}} \right)^2 \geq \mu_i \cdot \left(\sum_{j \in \vec{\mathcal{S}}_i} \frac{Q_{ij}}{\mu_i} \cdot \frac{Q_{ij}^\theta}{Q_{ij}} \right)^2 = \frac{1}{\mu_i} \cdot \left(\sum_{j \in \vec{\mathcal{S}}_i} Q_{ij}^\theta \right)^2 = \frac{(\mu_i^\theta)^2}{\mu_i},$$

where the inequality follows from Jensen's inequality. Combining the above two display equations, we can conclude that, indeed, $\bar{\psi}_{\mathbf{Q}}^{\theta\theta}(\theta) \geq 0$.

APPENDIX D

PROOF OF PROPOSITION 3

Maximizing $\psi_{\tilde{\mathbf{Q}}}(\mathbf{Q})$ over $\mathbf{Q} \in \mathcal{Q}(\mathcal{B})$ means to optimize a differentiable, concave function over a polytope. We therefore set up the Lagrangian

$$L \triangleq \sum_{(i,j) \in \mathcal{B}} Q_{ij} \cdot (\tilde{T}_{ij}^{\text{B}} - \tilde{T}_{ij}^{\text{E}}) - \bar{\psi}_{\tilde{\mathbf{Q}}}(\mathbf{Q}) + \lambda \cdot \left(\sum_{(i,j) \in \mathcal{B}} Q_{ij} - 1 \right) + \sum_{(i,j) \in \mathcal{B}} \lambda_j Q_{ij} - \sum_{(i,j) \in \mathcal{B}} \lambda_i Q_{ij}.$$

Note that at this stage we omit Lagrangian multipliers w.r.t. the constraints $Q_{ij} \geq 0$, $(i,j) \in \mathcal{B}$. We will make sure at a later stage that these constraints are satisfied thanks to the choice of κ in (15).

Recall that we assume that the surrogate function takes on its maximal value at $\mathbf{Q} = \mathbf{Q}^*$. Therefore, setting the gradient of L equal to the zero vector at $\mathbf{Q} = \mathbf{Q}^*$, we obtain

$$\begin{aligned} 0 &= \left. \frac{\partial L}{\partial Q_{ij}} \right|_{\mathbf{Q}=\mathbf{Q}^*} = \tilde{T}_{ij}^{\text{B}} - \tilde{T}_{ij}^{\text{E}} - \left. \frac{\partial \bar{\psi}_{\tilde{\mathbf{Q}}}(\mathbf{Q})}{\partial Q_{ij}} \right|_{\mathbf{Q}=\mathbf{Q}^*} + \lambda^* + \lambda_j^* - \lambda_i^*, \quad (i,j) \in \mathcal{B}, \quad (19) \\ 0 &= \left. \frac{\partial L}{\partial \lambda} \right|_{\mathbf{Q}=\mathbf{Q}^*} = \sum_{(i,j) \in \mathcal{B}} Q_{ij}^* - 1, \end{aligned}$$

$$0 = \frac{\partial L}{\partial \lambda_i} \Big|_{\mathbf{Q}=\mathbf{Q}^*} = \sum_{r \in \vec{\mathcal{S}}_i} Q_{ri}^* - \sum_{j \in \vec{\mathcal{S}}_i} Q_{ij}^*, \quad i \in \mathcal{S},$$

where

$$\begin{aligned} \frac{\partial \bar{\psi}_{\mathbf{Q}}(\mathbf{Q})}{\partial Q_{ij}} \Big|_{\mathbf{Q}=\mathbf{Q}^*} &= \kappa' \cdot \left(\kappa \cdot \log(1 + \kappa \cdot (\delta Q)_{ij}) - \kappa \cdot \log(1 + \kappa \cdot (\delta \mu)_i) \right) \Big|_{\mathbf{Q}=\mathbf{Q}^*} \\ &= \kappa \cdot \kappa' \cdot \log \left(\frac{(1 - \kappa) \cdot \tilde{Q}_{ij} + \kappa \cdot Q_{ij}^*}{(1 - \kappa) \cdot \tilde{\mu}_i + \kappa \cdot \mu_i^*} \cdot \frac{\tilde{\mu}_i}{Q_{ij}} \right) \\ &= \kappa \cdot \kappa' \cdot \log \left(\frac{\hat{Q}_{ij}^*}{\hat{\mu}_i^*} \cdot \frac{\tilde{\mu}_i}{\tilde{Q}_{ij}} \right) = \kappa \cdot \kappa' \cdot \log(\hat{p}_{ij}^*) - \kappa \cdot \kappa' \cdot \log(\tilde{p}_{ij}). \end{aligned} \quad (20)$$

Here the third and the fourth equality use $\{\hat{Q}_{ij}^*\}_{(i,j) \in \mathcal{B}}$, which is defined by

$$\hat{Q}_{ij}^* \triangleq (1 - \kappa) \cdot \tilde{Q}_{ij} + \kappa \cdot Q_{ij}^*, \quad (i, j) \in \mathcal{B}, \quad (21)$$

along with $\{\hat{\mu}_i^*\}_{i \in \mathcal{S}}$ and $\{\hat{p}_{ij}^*\}_{(i,j) \in \mathcal{B}}$, which are derived from $\{\hat{Q}_{ij}^*\}_{(i,j) \in \mathcal{B}}$ in the usual manner.

Note that $\hat{\mu}_i^* \triangleq \sum_{j' \in \vec{\mathcal{S}}_i} \hat{Q}_{ij'}^* = (1 - \kappa) \cdot \tilde{\mu}_i + \kappa \cdot \mu_i^*$, for all $i \in \mathcal{S}$, and

$$\hat{p}_{ij}^* = \frac{\hat{Q}_{ij}^*}{\hat{\mu}_i^*} = \frac{(1 - \kappa) \cdot \tilde{Q}_{ij} + \kappa \cdot Q_{ij}^*}{(1 - \kappa) \cdot \tilde{\mu}_i + \kappa \cdot \mu_i^*} = \frac{(1 - \kappa) \cdot \tilde{Q}_{ij} + \kappa \cdot Q_{ij}^*}{(1 - \kappa) \cdot \tilde{\mu}_i + \kappa \cdot \sum_{j' \in \vec{\mathcal{S}}_i} Q_{ij'}^*}, \quad (i, j) \in \mathcal{B}. \quad (22)$$

Note also that solving (21) for Q_{ij}^* results in $Q_{ij}^* = \frac{1}{\kappa} \cdot (\hat{Q}_{ij}^* - \tilde{Q}_{ij} + \kappa \cdot \tilde{Q}_{ij})$, $(i, j) \in \mathcal{B}$, which shows that $Q_{ij}^* \geq 0$, $(i, j) \in \mathcal{B}$, for κ satisfying (15). (Recall that when setting up the Lagrangian, we omitted the Lagrange multipliers for the constraints $Q_{ij} \geq 0$, $(i, j) \in \mathcal{B}$; therefore we have to verify that the solution satisfies these constraints, which it does indeed.)

Combining (19) and (20), and solving for \hat{p}_{ij}^* results in

$$\hat{p}_{ij}^* = \tilde{p}_{ij} \cdot \exp \left(\frac{\tilde{T}_{ij}^{\text{B}} - \tilde{T}_{ij}^{\text{E}} + \lambda^* + \lambda_j^* - \lambda_i^*}{\kappa \kappa'} \right), \quad (i, j) \in \mathcal{B}.$$

Using (13) and defining $\rho \triangleq \exp\left(-\frac{\lambda^*}{\kappa \kappa'}\right)$ and $\gamma = \left(\gamma_i \triangleq \exp\left(\frac{\lambda_i^*}{\kappa \kappa'}\right)\right)_{i \in \mathcal{S}}$, allows the rewriting of this equation as $\hat{p}_{ij}^* = \frac{A_{ij}}{\rho} \cdot \frac{\gamma_j}{\gamma_i}$, $(i, j) \in \mathcal{B}$. Because $\sum_{j \in \vec{\mathcal{S}}_i} \hat{p}_{ij}^* = 1$ for all $i \in \mathcal{S}$, summing both sides of this equation over $j \in \vec{\mathcal{S}}_i$ results in $1 = \sum_{j \in \vec{\mathcal{S}}_i} \frac{A_{ij}}{\rho} \cdot \frac{\gamma_j}{\gamma_i}$, $i \in \mathcal{S}$, or, equivalently, $\rho \cdot \gamma_i = \sum_{j \in \vec{\mathcal{S}}_i} A_{ij} \cdot \gamma_j$, $i \in \mathcal{S}$. This system of linear equations can be written as $\mathbf{A} \cdot \boldsymbol{\gamma} = \rho \cdot \boldsymbol{\gamma}$. Clearly, this equation can only be satisfied if $\boldsymbol{\gamma}$ is an eigenvector of \mathbf{A} with corresponding eigenvalue ρ . A slightly lengthy calculation (which is somewhat similar to the calculation

in [21, Eq. (51)]) shows that $\psi_{\mathbf{Q}}(\mathbf{Q}^*) = \log(\rho)$. Clearly, in order to maximize $\log(\rho)$ over all eigenvalues of \mathbf{A} , the eigenvalue ρ has to be the Perron–Frobenius eigenvalue and $\boldsymbol{\gamma}$ the corresponding eigenvector.

The proof is concluded by noting that (22) can be rewritten as the system of linear equations $Q_{ij}^* - \hat{P}_{ij}^* \cdot \sum_{j' \in \vec{\mathcal{S}}_i} Q_{ij'}^* = \frac{1-\kappa}{\kappa} \cdot (\tilde{\mu}_i \hat{P}_{ij}^* - \tilde{Q}_{ij})$, $(i, j) \in \mathcal{B}$, which can be used to determine $\{Q_{ij}^*\}_{(i,j) \in \mathcal{B}}$, because all other quantities appearing in these equations are either known or have already been calculated.

REFERENCES

- [1] A. Nouri, R. Asvadi, J. Chen, and P. O. Vontobel, “Finite-input intersymbol interference wiretap channels,” in *Proc. IEEE Inf. Theory Workshop*, Kanazawa, Japan, Oct. 17–21 2021, pp. 1–6.
- [2] Y. Liu, H. H. Chen, and L. Wang, “Physical layer security for next generation wireless networks: Theories, technologies, and challenges,” *IEEE Commun. Surv. Tutor.*, vol. 19, no. 1, pp. 347–376, 1st Quart., 2017.
- [3] C. Gidney and M. Ekerå, “How to factor 2048 bit RSA integers in 8 hours using 20 million noisy qubits,” *Quantum*, vol. 5, p. 433, Apr. 2021.
- [4] M. Bloch, O. Günlü, A. Yener, F. Oggier, H. V. Poor, L. Sankar, and R. F. Schaefer, “An overview of information-theoretic security and privacy: metrics, limits and applications,” *IEEE J. Sel. Areas Inf. Theory*, vol. 2, no. 1, pp. 5–22, Mar. 2021.
- [5] J. M. Hamamreh, H. M. Furqan, and H. Arslan, “Classifications and applications of physical layer security techniques for confidentiality: A comprehensive survey,” *IEEE Commun. Surv. Tutor.*, vol. 21, no. 2, pp. 1773–1828, 2nd Quart., 2019.
- [6] J. G. Proakis and M. Salehi, *Digital Communications 5th Edition*. McGraw Hill, 2008.
- [7] L. Zhang, A. Ijaz, P. Xiao, and R. Tafazolli, “Channel equalization and interference analysis for uplink narrowband internet of things (NB-IoT),” *IEEE Commun. Lett.*, vol. 21, no. 10, pp. 2206–2209, May 2017.
- [8] J. Choi, “Single-carrier index modulation for IoT uplink,” *IEEE J. Sel. Top. Signal Process.*, vol. 13, no. 6, pp. 1237–1248, Oct. 2019.
- [9] European Telecommunications Standards Institute, “Evolved universal terrestrial radio access (E-UTRAN): Physical channels and modulation,” *ETSI TS 136 211 V16.5.0*, May 2021.
- [10] C. Kuhlins, B. Rathonyi, A. Zaidi, and M. Hogan, “Cellular networks for massive IoT,” *Ericsson White Paper Uen 284 23-3278*, Jan. 2020.
- [11] Y. Cao, W. Shi, L. Sun, and X. Fu, “Channel state information-based ranging for underwater acoustic sensor networks,” *IEEE Trans. Wirel. Commun.*, vol. 20, no. 2, pp. 1293–1307, Feb. 2021.
- [12] B. Dai, Z. Ma, Y. Luo, X. Liu, Z. Zhuang, and M. Xiao, “Enhancing physical layer security in internet of things via feedback: A general framework,” *IEEE Internet Things J.*, vol. 7, no. 1, pp. 99–115, Jan. 2020.
- [13] J. Zhang, S. Rajendran, Z. Sun, R. Woods, and L. Hanzo, “Physical layer security for the internet of things: Authentication and key generation,” *IEEE Wirel. Commun.*, vol. 26, no. 5, pp. 92–98, Oct. 2019.

- [14] S. Jiang, “On securing underwater acoustic networks: A survey,” *IEEE Commun. Surv. Tutor.*, vol. 21, no. 1, pp. 729–752, 1st Quart., 2019.
- [15] European Telecommunications Standards Institute, “LTE; evolved universal terrestrial radio access (E-UTRA): User equipment (UE) radio transmission and reception,” *ETSI TS 136 101 V16.9.0 Release 16*, May 2021.
- [16] J. Ma, R. Shrestha, J. Adelberg, C. Y. Yeh, Z. Hossain, E. Knightly, J. M. Jornet, and D. M. Mittleman, “Security and eavesdropping in terahertz wireless links,” *Nature*, vol. 563, pp. 89–93, Oct. 2018.
- [17] T. M. Duman and M. Stojanovic, “Information rates of energy harvesting communications with intersymbol interference,” *IEEE Commun. Lett.*, vol. 23, no. 12, pp. 2164–2167, Dec. 2019.
- [18] R. G. Gallager, *Information Theory and Reliable Communication*. New York, NY, USA: John Wiley & Sons, 1968.
- [19] R. Blahut, “Computation of channel capacity and rate-distortion functions,” *IEEE Trans. Inf. Theory*, vol. 18, no. 4, pp. 460–473, July 1972.
- [20] S. Arimoto, “An algorithm for computing the capacity of arbitrary discrete memoryless channels,” *IEEE Trans. Inf. Theory*, vol. 18, no. 1, pp. 14–20, Jan. 1972.
- [21] P. O. Vontobel, A. Kavčić, D. M. Arnold, and H. A. Loeliger, “A generalization of the Blahut-Arimoto algorithm to finite-state channels,” *IEEE Trans. Inf. Theory*, vol. 54, no. 5, pp. 1887–1918, May 2008.
- [22] A. Kavčić, “On the capacity of Markov sources over noisy channels,” in *Proc. IEEE Glob. Commun. Conf.*, vol. 5, San Antonio, TX, USA, Nov. 2001, pp. 2997–3001.
- [23] S. Yang, A. Kavčić, and S. Tatikonda, “Feedback capacity of finite-state machine channels,” *IEEE Trans. Inf. Theory*, vol. 51, no. 3, pp. 799–810, Mar. 2005.
- [24] P. O. Vontobel and D. M. Arnold, “An upper bound on the capacity of channels with memory and constraint input,” in *Proc. IEEE Inf. Theory Workshop*, Cairns, Queensland, Australia, Sept. 2001, pp. 147–149.
- [25] J. Chen and P. H. Siegel, “Markov processes asymptotically achieve the capacity of finite-state intersymbol interference channels,” *IEEE Trans. Inf. Theory*, vol. 54, no. 3, pp. 1295–1303, Mar. 2008.
- [26] T. S. Han and M. Sasaki, “Wiretap channels with causal state information: Strong secrecy,” *IEEE Trans. Inf. Theory*, vol. 65, no. 10, pp. 6750–6765, Oct. 2019.
- [27] —, “Wiretap channels with causal and non-causal state information: Revisited,” *IEEE Trans. Inf. Theory*, vol. 67, no. 9, pp. 6122 – 6139, Sept. 2021.
- [28] B. Dai, C. Li, Y. Liang, Z. Ma, and S. Shamai (Shitz), “Impact of action-dependent state and channel feedback on Gaussian wiretap channels,” *IEEE Trans. Inf. Theory*, vol. 66, no. 6, pp. 3435–3455, June 2020.
- [29] B. Dai, Z. Ma, and Y. Luo, “Finite state Markov wiretap channel with delayed feedback,” *IEEE Trans. Inf. Forensics Secur.*, vol. 12, no. 3, pp. 746–760, Mar. 2017.
- [30] S. Hanoglu, S. R. Aghdam, and T. M. Duman, “Artificial-noise-aided secure transmission over finite-input intersymbol interference channels,” in *Proc. 25th Int. Conf. Telecommun.*, Saint-Malo, France, June 2018, pp. 346–350.
- [31] J. de Dieu Mutangana and R. Tandon, “Blind MIMO cooperative jamming: secrecy via ISI heterogeneity without CSIT,” *IEEE Trans. Inf. Forensics Secur.*, vol. 15, pp. 447–461, 2020.
- [32] Y. Sankarasubramaniam, A. Thangaraj, and K. Viswanathan, “Finite-state wiretap channels: Secrecy under memory constraints,” in *Proc. IEEE Inf. Theory Workshop*, Taormina, Italy, Oct. 2009, pp. 115–119.

- [33] I. Csiszár and J. Körner, “Broadcast channels with confidential messages,” *IEEE Trans. Inf. Theory*, vol. 24, no. 3, pp. 339–348, May 1978.
- [34] D. M. Arnold, H. A. Loeliger, P. O. Vontobel, A. Kavčić, and W. Zeng, “Simulation-based computation of information rates for channels with memory,” *IEEE Trans. Inf. Theory*, vol. 52, no. 8, pp. 3498–3508, Aug. 2006.
- [35] A. Kavčić, X. Ma, and N. Varnica, “Matched information rate codes for partial response channels,” *IEEE Trans. Inf. Theory*, vol. 51, no. 3, pp. 973–989, Mar. 2005.
- [36] A. Nouri and R. Asvadi, “Matched information rate codes for binary-input intersymbol interference wiretap channels,” in *Proc. IEEE Int. Symp. Inf. Theory*, Espoo, Finland, June 2022, pp. 1163–1168.
- [37] U. M. Maurer, “The strong secret key rate of discrete random triples,” in *Title: Communications and Cryptography: Two Sides of One Tapestry*. Boston, MA: Springer US, 1994, pp. 271–285.
- [38] A. D. Wyner, “The wire-tap channel,” *Bell Syst. Tech. J.*, vol. 54, no. 8, pp. 1355–1387, Oct. 1975.
- [39] M. Bloch and J. Barros, *Physical-Layer Security: From Information Theory to Security Engineering*, 1st ed. New York, NY, USA: Cambridge University Press, 2011.
- [40] M. Bloch and J. N. Laneman, “Strong secrecy from channel resolvability,” *IEEE Trans. Inf. Theory*, vol. 59, no. 12, pp. 8077–8098, Dec. 2013.
- [41] M. Bellare, S. Tessaro, and A. Vardy, “Semantic security for the wiretap channel,” in *Proc. CRYPTO 2012*, vol. 7417, Berlin, Heidelberg, 2012, pp. 294–311.
- [42] T. S. Han, *Information-Spectrum Methods in Information Theory*. Berlin, Heidelberg, New York: Springer, 2003.
- [43] M. Bloch and J. N. Laneman, “On the secrecy capacity of arbitrary wiretap channels,” in *Proc. 46th Annual Allerton Conf. Commun. Control and Computing*, Monticello, IL, USA, Sept. 2008, pp. 818–825.
- [44] P. Sadeghi, P. O. Vontobel, and R. Shams, “Optimization of information rate upper and lower bounds for channels with memory,” *IEEE Trans. Inf. Theory*, vol. 55, no. 2, pp. 663–688, Feb. 2009.
- [45] A. P. Dempster, N. M. Laird, and D. B. Rubin, “Maximum likelihood from incomplete data via the EM algorithm,” *J. R. Stat. Soc. Ser. B (Methodological)*, pp. 1–38, 1977.
- [46] C. F. J. Wu, “On the convergence properties of the EM algorithm,” *Ann. Stat.*, vol. 11, no. 1, pp. 95–103, Mar. 1983.
- [47] G. L. Stüber, *Principles of Mobile Communication*, 4th ed. Cham, Switzerland: Springer International Publishing, 2017.
- [48] W. Xiang and S. Pietrobon, “On the capacity and normalization of ISI channels,” *IEEE Trans. Inf. Theory*, vol. 49, no. 9, pp. 2263–2268, Sept. 2003.
- [49] A. Chakrapani, “NB-IoT uplink receiver design and performance study,” *IEEE Internet Things J.*, vol. 7, no. 3, pp. 2469–2482, Mar. 2020.
- [50] K. L. Judd, *Numerical Methods in Economics*. London, UK: The MIT Press, 1998.
- [51] A. Nouri, “ISI Wiretap Channels [SIMULATION_FILES],” Oct. 2021. [Online]. Available: <https://doi.org/10.5281/zenodo.5595240>
- [52] S. K. Leung-Yan-Cheong and M. E. Hellman, “The Gaussian wire-tap channel,” *IEEE Trans. Inf. Theory*, vol. 24, no. 4, pp. 451–456, Jul. 1978.